Economic Geology
Vol. 85, 1990, pp. 1738–1758

Evolution of the Monte Negro Acid Sulfate Au-Ag Deposit, Pueblo Viejo, Dominican Republic: Important Factors in Grade Development

JOHN L. MUNTEAN,* STEPHEN E. KESLER,

Department of Geological Sciences, University of Michigan, Ann Arbor, Michigan 48109

NORMAN RUSSELL, AND JOSE POLANCO

Rosario Dominicana, S.A., P.O. Box 944, Santo Domingo, Dominican Republic

Abstract

This study was undertaken to determine the geologic factors that were important in making Pueblo Viejo, which contains over 600,000 kg of gold in relatively high-grade ore, one of the few acid sulfate deposits to be mined economically on a large scale. Orebodies at Pueblo Viejo, including Monte Negro, the focus of this study, are found around a maar-diatreme complex that formed in the upper part of the Lower Cretaceous Los Ranchos Formation. Ore is hosted by spilite, spilite-derived conglomerate, and intramaar carbonaceous sandstone and mudstone. Regional seawater alteration of these rocks was overprinted by two stages of advanced argillic alteration, both of which are associated with precious metals. Stage I produced deep alunite + quartz + pyrite and overlying kaolinite + quartz + pyrite assemblages and deposited gold in association with disseminated pyrite in wall rock. Stage II, which overprinted stage I, produced deep pyrophyllite ± diaspore and an overlying (recrystallized) silica cap. Pyrite ± sphalerite ± enargite veins that probably formed in response to hydrofracturing of the silica cap contain gold grades of as much as 100 ppm. Vein density and assay data show that approximately 60 percent of the gold at Monte Negro is in disseminated stage I ore, with the remainder in stage II veins.

Phase equilibria and sulfur isotope thermometry show that stage I alteration took place below 260°C at pH values between 2 and 3. Stage II pyrophyllite ± diaspore formation occurred above 285°C, from a fluid with an initial pH of 1 to 1.5, while the silica caps formed below 220°C. Geologic constraints indicate that stage I wall-rock gold at Monte Negro was deposited by sulfidation of Fe-rich wall rock, whereas stage II vein-hosted gold could have formed by cooling, boiling, or mixing with overlying ground water. Use of the programs SOLVEQ and CHILLER to evaluate the relative efficiencies of these ore-forming processes confirms that sulfidation was capable of depositing disseminated stage I gold, whereas stage II vein gold was probably deposited by boiling related to pressure release during hydrofracturing and subsequent mixing with ground water.

These observations indicate that development of grade and tonnage at Pueblo Viejo was greatly facilitated by (1) the porous-permeable maar-diatreme complex, which hosted large, shallow hydrothermal cells and probably served as a conduit for rising magmatic gases, (2) the presence of iron-rich wall rock, which caused early deposition of "background" disseminated gold by sulfidation, and (3) later hydrothermal activity which formed impermeable silica caps that hydrofractured to create the high-grade vein overprint. Remobilization of stage I background gold into stage II veins might also have been an important factor in upgrading the deposits. Exploration for similar deposits should focus on areas of explosive volcanism in andesitic island arc terranes.

Introduction

ALTHOUGH acid sulfate precious metal deposits are widespread (Heald et al., 1987), surprisingly few have the grade and tonnage required for large-scale bulk mining. Many deposits, including Goldfield (Ransome, 1909) and El Indio (Siddeley and Araneda, 1986), have been mined by selective methods, and in others, such as Summitville, where bulk mining methods have been applied, results have been discouraging. The most prominent exception to this rule, the Pueblo Viejo district in the Dominican Republic, has produced over 50 metric tons of oxide ore grading approximately 4 ppm, all of which has been extracted by open-pit bulk mining methods at a rate of about 10,000 metric tons per day. Approximately 100 million metric tons of slightly lower grade sulfide ore, which is also amenable to bulk mining, underlies the oxide ore in the deposits at Pueblo Viejo. This report, which focuses on the Monte Negro deposit, the sec-

* Present address: Santa Fe Pacific Mining, Inc., 250 S. Rock Blvd., Suite 100, Reno, Nevada 89502.

0361-0128/90/1150/1738-21$3.00

ond largest orebody at Pueblo Viejo, was undertaken to identify the geologic factors that permitted Pueblo Viejo to be an economic success.

Geologic Setting of Pueblo Viejo Mineralization

Pueblo Viejo is in the upper part of the Lower Cretaceous Los Ranchos Formation, a series of volcanic and volcaniclastic rocks on the east side of the Cordillera Central, the axial mountain range of Hispaniola (Bowin, 1966). The Los Ranchos Formation consists of a lower complex of pillowed spilite flows and keratophyre and quartz keratophyre flows, tuffs, and intrusions, which are overlain by volcaniclastic sediments and lahars. These are overlain, in turn, by an extensive spilite unit that lacks pillows and contains lenses of sediment with plant fossils (Kesler et al., 1991). A maar-diatreme complex in the upper part of the Los Ranchos Formation, which formed during the latest phase of volcanism, hosts the Pueblo Viejo district (Sillitoe and Bonham, 1984; Russell and Kesler, 1991). The complex includes fragmented spilite, redeposited pyroclastic rocks, quartz eye-bearing lapilli tuff, and carbonaceous lacustrine sediments (Figs. 1 and 2).

Primary magmatic minerals in the Los Ranchos Formation have been almost entirely altered to albite, quartz, calcite, chlorite, illite, smectite, epidote, actinolite, and prehnite. Evidence that these minerals were produced by seawater alteration rather than as a propylitic halo related to Pueblo Viejo mineralization is indicated by strontium isotope compositions of calcite in amygdules, which are similar to Cretaceous seawater (Kesler et al., 1991).

The Pueblo Viejo district comprises several acid sulfate orebodies, of which Moore and Monte Negro are the two largest (Fig. 2). The deposits are found at or near the margin of the maar-diatreme complex, where they form mushroom-shaped bodies that overprint the regional seawater alteration. Monte Negro, which is found along the western margin of the maar-diatreme complex contains 14 million metric tons of oxide ore grading 3.35 ppm gold and 7.6 ppm silver (0.8 ppm gold cutoff), which overlies a 37-million-metric-ton sulfide reserve, grading 3.95 ppm gold and 22.4 ppm silver (2.5 ppm gold cutoff) (Russell et al.,

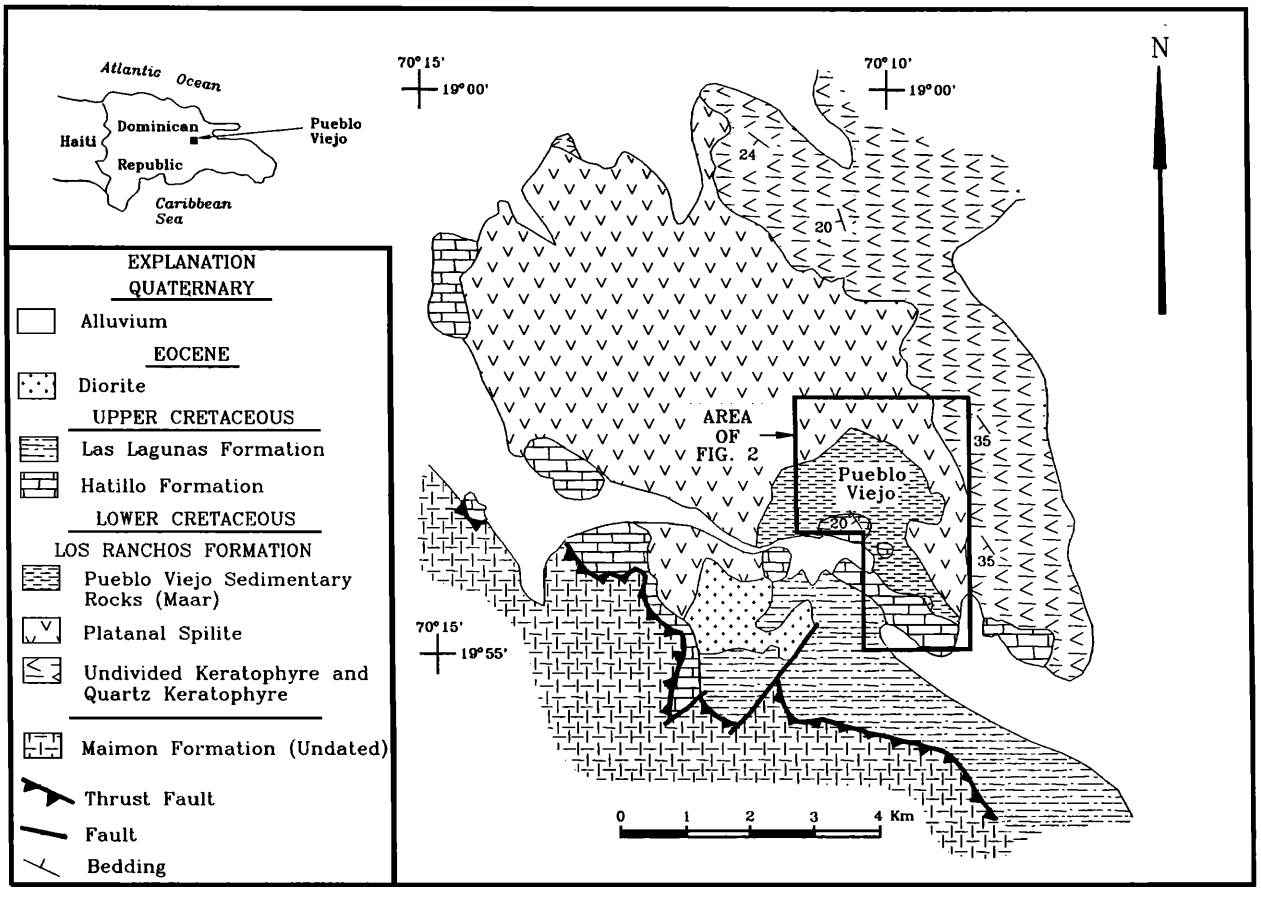

FIG. 1. Geologic map of the central Los Ranchos Formation (after Kesler et al., 1990).

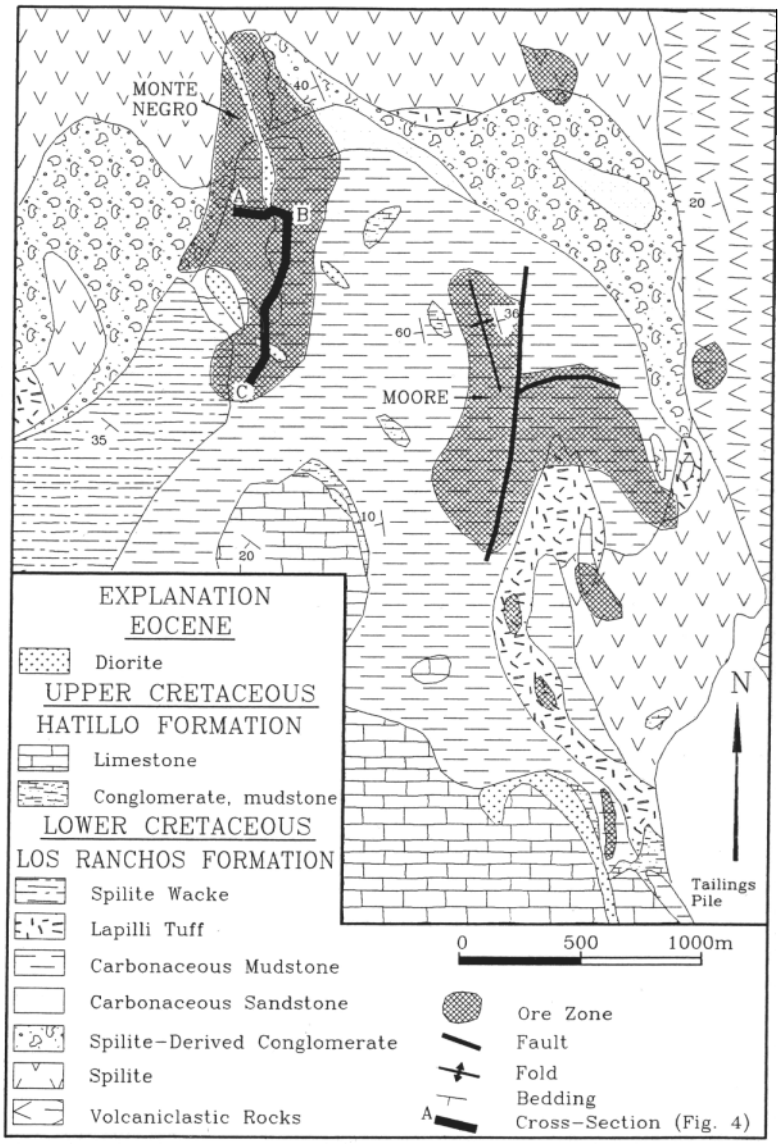

FIG. 2. Geologic map of the maar-diatreme complex at Pueblo Viejo showing locations of the Monte Negro and Moore orebodies (after Russell et al., 1990).

1981). The Monte Negro orebody is restricted in volume in the spilite but spreads out in the overlying intramaar sedimentary rocks. The orebody is largely undeformed and is cut by postore, Eocene (?) diorite dikes. Although alunite from the Moore orebody yields a 66-Ma $^{40}Ar/^{39}Ar$ age (Kesler et al., 1981), geologic and fossil evidence strongly points to a Lower Cretaceous age for the mineralization (Russell and Kesler, 1991).

Zoning and Paragenesis of Advanced Argillic Alteration and Precious Metal Mineralization

Introduction

Two stages of advanced argillic alteration and associated precious metal mineralization that are complexly zoned both spatially and temporally have been delineated at Monte Negro. Stage I is characterized by the complete replacement of the regional seawater alteration by a zoned sequence of advanced argillic alteration consisting of deep alunite-quartz-pyrite-rutile, which underlies a more extensive kaolinite-quartz-pyrite-rutile zone. Disseminated gold is associated with wall-rock pyrite and is believed to have been deposited during formation of the kaolinite zone. Stage II advanced argillic alteration, which is characterized by widespread pyrophyllite ± diaspore and high-level caps of massive silicification, has overprinted and replaced stage I alteration to varying degrees. High-grade gold-bearing sulfide veins were emplaced during stage II, probably in response to hy-

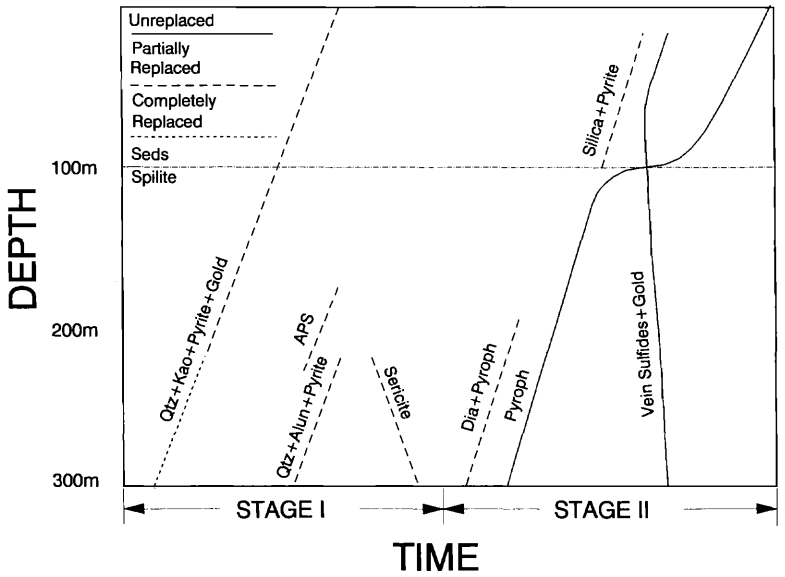

FIG. 3. Paragenetic diagram showing temporal and depth zoning of mineral assemblages. Depths are approximate. Positive slopes indicate prograde assemblages, while negative slopes indicate retrograde assemblages. APS = alumino-phosphate-sulfate minerals, Dia = diaspore, Kao = kaolinite, Pyroph = pyrophyllite, Qtz = quartz, Silica = recrystallized metastable silica phases.

drofracturing of the high-level silica caps. Figure 3, which is a paragenetic diagram, Figure 4, which is a series of cross sections showing geology, alteration, grade distribution, and Figure 5, which is a series of photomicrographs showing key paragenetic relationships, attempt to illustrate this spatial and temporal zonation of alteration and mineralization and should be referred to as detailed descriptions of the alteration and mineralization presented below.

Stage I alteration and mineralization

In spilite and spilite-derived conglomerate the kaolinite-quartz-pyrite-rutile zone contains pseudomorphic patches of kaolinite in what were once feldspar phenocryst sites. Other phenocryst sites which were probably mafic minerals contain quartz, pyrite, and rutile. The altered groundmass consists of cloudy, fine-grained, anhedral quartz with disseminated pyrite and rutile. In the lacustrine sandstone and mudstone, kaolinite is much less common and occurs as irregular masses, and siderite is replaced by pyrite.

There is a sharp transition, over a few meters (Fig. 4B), from kaolinite-bearing rocks to an underlying zone containing phenocryst sites that are occupied by clear quartz and alunite in a groundmass of fine-grained (<50 μm) anhedral quartz, alunite, pyrite, and rutile. This alunite zone, which is entirely in spilite, hosts veinlets of quartz, alunite, and pyrite that exhibit mutual equilibrium textures (Fig. 5A) and appear to be contemporaneous with the wall-rock alteration. Microprobe analyses of the alunite show a range of Na/(Na + K) mole ratios (0.2–0.8, Table 1) both in the wall rock and veinlets. These compositions suggest solid solution between alunite and natroalunite, despite experimental data (Stoffregen, 1988) permitting an assymetric solvus below 350°C. The alunite shows no spatial or temporal compositional zoning, and the observed range of compositions could reflect multiple pulses of fluid of slightly different compositions during the formation of the alunite zone or, more likely, retrograde reaction of alunite with later fluids.

Aluminophosphate-sulfate minerals, including svanbergite and woodhouseite, are located along the periphery of the alunite zone. These minerals are not directly associated with either alunite or kaolinite and occur with quartz as discrete euhedral to subhedral grains (<50 μm) in the wall rock or more rarely as veinlets with no alteration envelopes. Although they could be partly the result of apatite replacement (Stoffregen and Alpers, 1987), local introduction of phosphorous is needed to account for zones containing as much as 5 percent of these minerals.

Inclusions of gold-rich electrum and tellurides, as well as Cu-As-Pb-Ag sulfides, have been recognized in pyrite framboids and euhedra in the wall rock in the kaolinite zone and are believed to have formed during stage I sulfidation of wall rock in the kaolinite zone (Kettler, 1989).

Retrograding of stage I alteration, which is indicated by local replacement of alunite by sericite, suggests that the stage I thermal event decayed before the beginning of stage II alteration and mineralization.

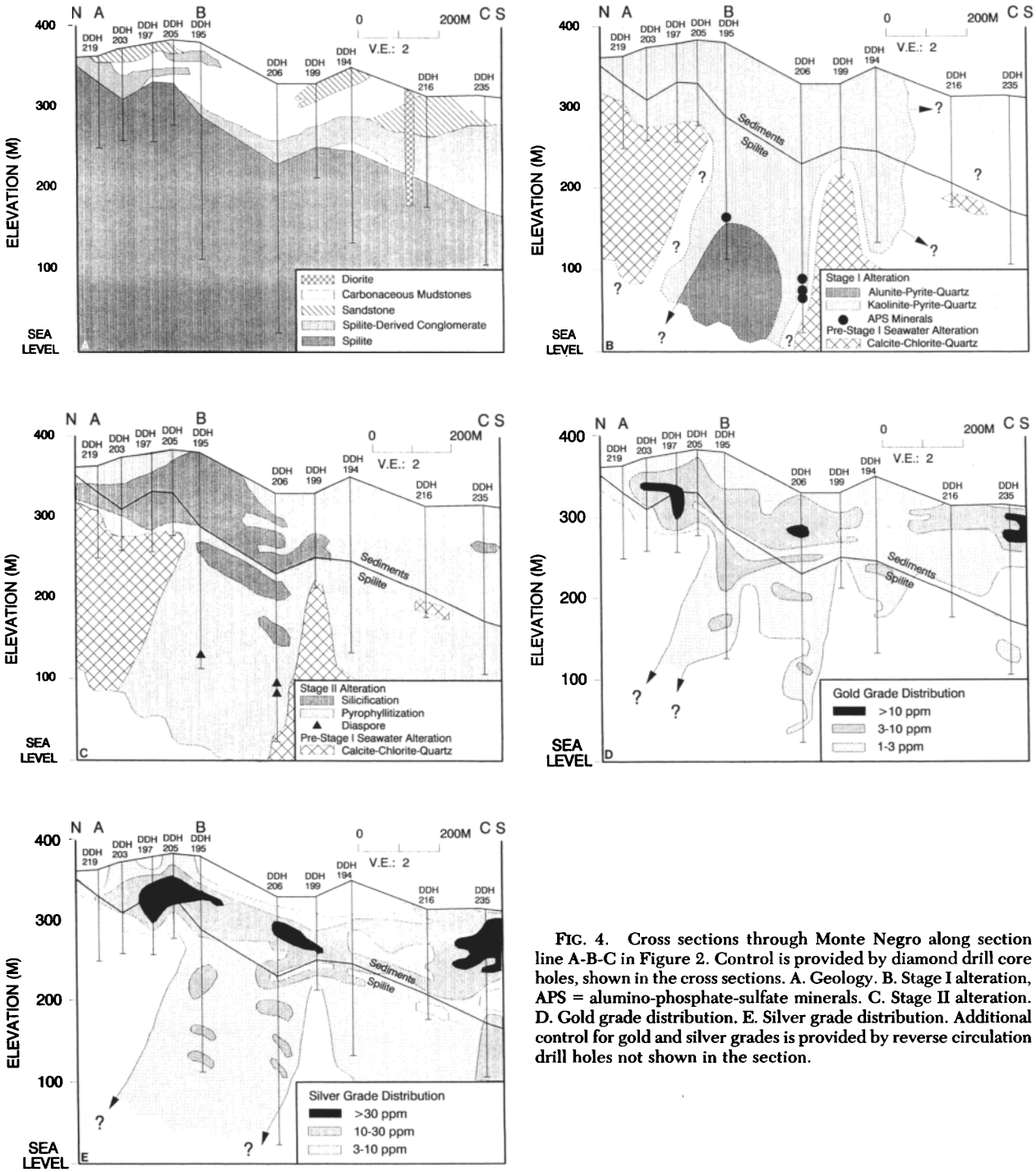

FIG. 4. Cross sections through Monte Negro along section line A-B-C in Figure 2. Control is provided by diamond drill core holes, shown in the cross sections. A. Geology. B. Stage I alteration, APS = alumino-phosphate-sulfate minerals. C. Stage II alteration. D. Gold grade distribution. E. Silver grade distribution. Additional control for gold and silver grades is provided by reverse circulation drill holes not shown in the section.

Stage II alteration and mineralization

Stage II alteration is characterized by widespread pyrophyllite ± diaspore, high-level caps of massive silicification, and associated gold-bearing sulfide veins (Fig. 4C). Petrographic evidence, discussed below, suggests that stage II is a distinct, later event that has overprinted and replaced stage I alteration to varying degrees. In the southern end of Monte Negro (Fig. 4C), the stage II alteration was so intense that no ves-

tiges of stage I alteration remain, and it is possible that some stage II alteration extended beyond stage I alteration.

Where stage II alteration overprinted the alunite zone of stage I, diaspore replaced alunite locally, and pyrophyllite formed veinlets and patches that cut alunite, quartz, and pyrite. Pyrophyllite content of the relict alunite zone reaches approximately 20 percent (by volume), but is usually much less. The fact that pyrophyllite also replaced stage I retrograde sericite locally indicates that stage II alteration was a distinct, later event after the collapse of the stage I system.

Incipient stage II overprinting of the kaolinite zone is characterized by monomineralic pyrophyillite veinlets that cut the quartz-rich matrix and coalesce at kaolinite patches, where pyrophyllite has replaced kaolinite to varying degrees (Fig. 5B). Further stage II overprinting resulted in the complete replacement of kaolinite and extensive replacement of quartz by pyrophyillite (Fig. 5C), leaving some zones in which pyrite and rutile are the only remaining stage I minerals. Little additional wall-rock pyrite appears to have been deposited during formation of stage II pyrophyllite, and the pyrite exhibits smooth grain boundaries with pyrophyllite, suggesting equilibrium between the two minerals during stage II.

Diaspore is present locally in deeper parts of the relict kaolinite zone that have undergone extensive replacement by pyrophyllite. It forms patches that appear to be in equilibrium with pyrophyllite (Fig. 5D) in some places and to be replaced by pyrophyllite in others. In deep parts of the relict kaolinite zone, replacement of stage I aluminophosphate-sulfate minerals by diaspore has also been observed.

Massive silica caps are found in the relict kaolinite zone above areas of massive pyrophyllite ± diaspore. They are most intense in the conglomeratic horizons that directly overlie the spilite where the rock consists almost entirely of microcrystalline quartz, similar to jasperoid. Pyrite, which is coarser than the finely disseminated pyrite described above for stage I, is abundant in the silicified rocks, although it is difficult to determine whether it was deposited along with silica. Minor enargite and sphalerite are also present but are not observed together or with pyrite. The massive silica is characterized in thin section by numerous overlapping veinlets consisting soley of clear quartz, which cut the stage I quartz-pyrite-rutile matrix. These veinlets coalesce at kaolinite patches, where coarse, clear quartz has replaced kaolinite (Fig. 5E).

Many textures in the silicified rocks resemble recrystallized silica, such as chalcedony, opal, or amorphous silica. Clear crosscutting quartz veinlets which are filled with fine-grained, anhedral quartz, show no development of crystals with the *c* axis perpendicular to the veinlet wall and are interpreted to have formed by recrystallization of amorphous silica (Fournier, 1985). Boundaries between cloudy and clear quartz, as observed under uncrossed polars, are transected by boundaries between quartz grains of uniform extinction when viewed under crossed polars (Fig. 5F and G). Plumose quartz, which may also be recrystallized metastable silica (Sander and Black, 1988), has been observed locally in the silicified rocks.

In the intensely silicified caps, the rock is cut by sharply walled veinlets of pyrophyllite. Kaolinite and minor amounts of silica have been replaced partly by pyrophyllite in the silicified rocks. Above the silicified zones, pyrophyllite has replaced both kaolinite and quartz extensively, much like the zone of massive pyrophyllite below the silicified caps. The amount of introduced stage II silica and the pervasiveness of pyrophyllite formation vary inversely.

Gold-bearing sulfide veins cut stage I and are interpreted to be contemporaneous with stage II alteration. The veins are commonly less than 2 cm thick and have sharp walls in the fine-grained sediments and more irregular boundaries in the conglomerate and spilite. Alteration selvages are uncommon, although cm-scale envelopes of silicification and, more rarely, pyrophyllite formation can be seen locally, and swarms of veins are closely associated with areas of intense silicification. Several episodes of veining are indicated by crosscutting veins of several different orientations, suggesting vein emplacement resulted from hydrofracturing.

The veins are distinctive in being rich in sulfides and poor in gangue minerals. Pyrite, by far the most common mineral in the veins, forms fine-grained, bi-

TABLE 1. Microprobe Determination of Na/(Na+K) Mole Ratios in Alunite

	1	2	3	4	5	6[1]	7[1]
Na/(Na+K)	0.649	0.417	0.399	0.792	0.795	0.205	0.197

Sample descriptions: 1, 2, 3 = DDH195, 246.9 m, wall-rock alunite directly next to pyrite-alunite-quartz veinlet; 4 = DDH195, 236.5 m, wall-rock alunite in phenocryst site; 5, 6, 7 = DDH195, 246.9 m, alunite from pyrite-alunite-quartz veinlet

[1] Analyses 6 and 7 were 20 μm apart on a single grain; other analyses were on separate grains

The alunite was analyzed with the Cameca electron microprobe at the University of Michigan using an accelerating voltage of 10 kV; natural standards were used, including Marysvale alunite (S, Al, K), jadeite (Na), barite (Ba), hornblende (Fe), celestite (Sr), and apatite (P); a diffuse beam (10–29 μm in diam) was used to minimize vaporization

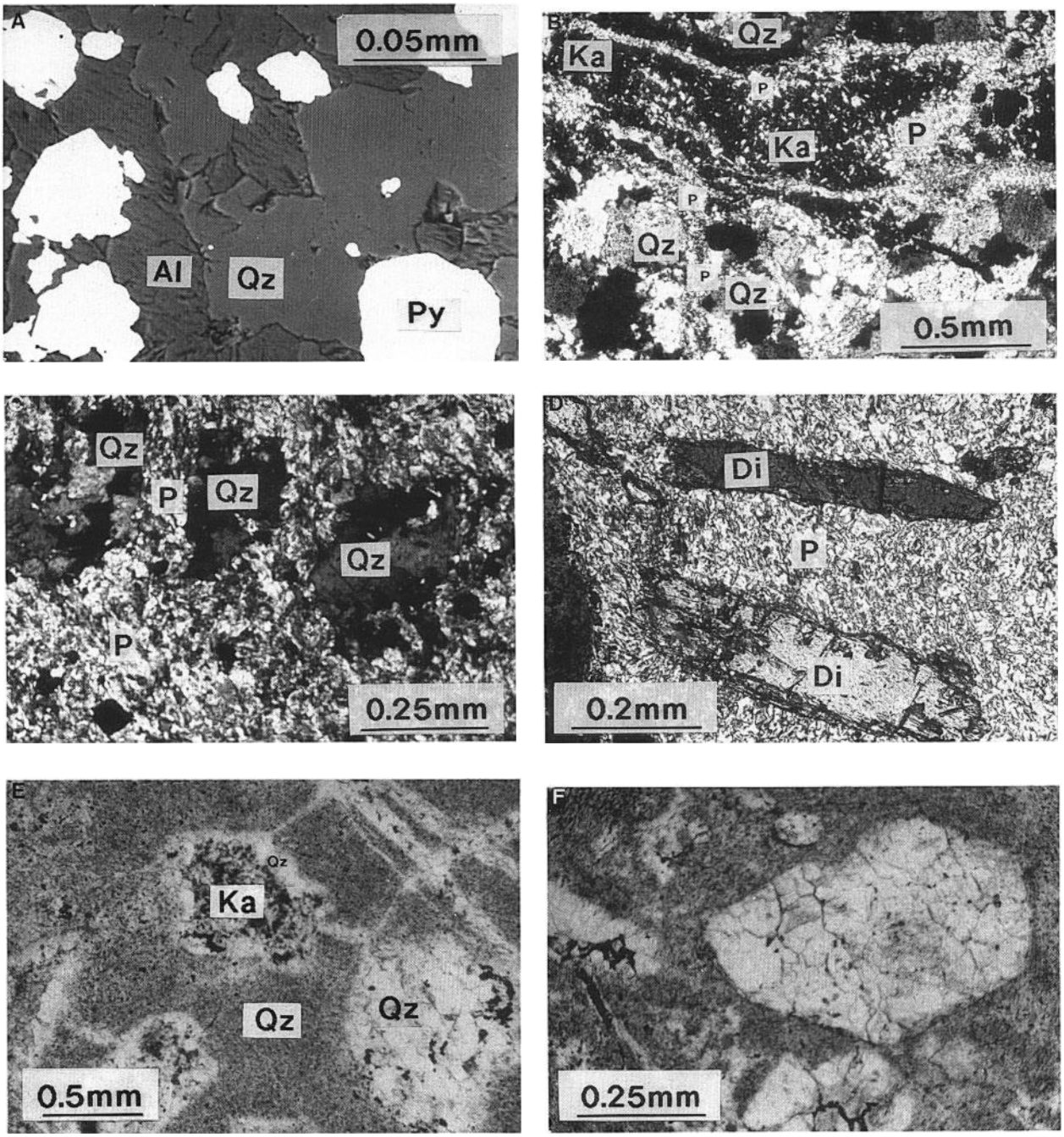

FIG. 5.

laterally symmetrical, colloform layers indicating open-space filling. The central parts of many veins are filled by enargite and sphalerite, with enargite more common in the central part of the orebody and sphalerite more common in peripheral parts of the deposit. Both enargite and sphalerite can form monomineralic veins and masses locally. Sphalerite is commonly color banded, although, microprobe analyses indicate no change in Fe, Mn, or Cd with color. The Fe content of the sphalerite is low, with mole percent FeS ranging from nondetectable levels to 0.38 percent. Other, less abundant, sulfide-sulfosalt vein minerals include Zn-bearing tennantite (actually tennantite-tetrahedrite with As/Sb mole ratios ranging from

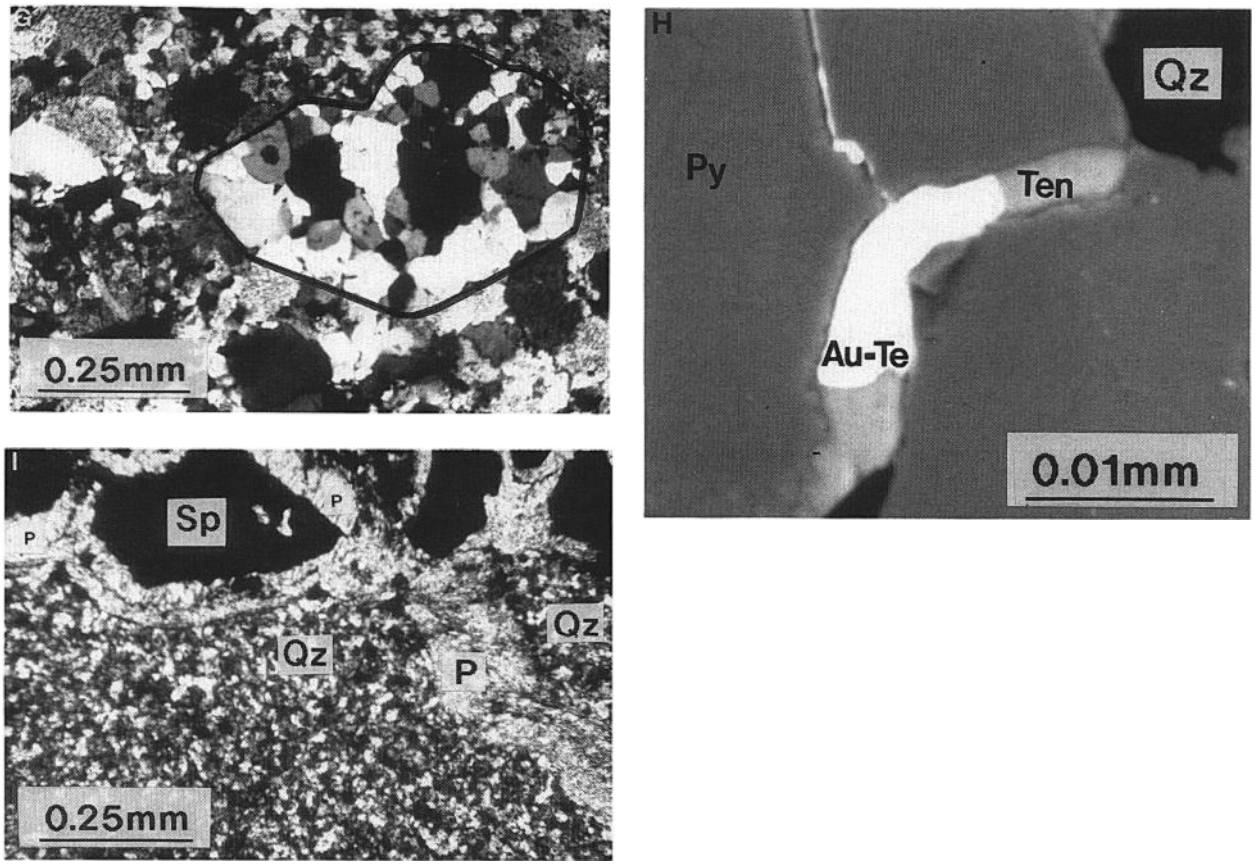

FIG. 5. Photomicrographs illustrating paragenetic relationships. A. Back-scattered electron image of sample from alunite zone showing an equilibrium intergrowth between alunite, pyrite, and quartz in a veinlet. B. Pyrophyllite (light, fine-grained material) crosscutting and replacing kaolinite patch (dark material). Pyrophyllite is also crosscutting quartz in discrete veinlets. Crossed polars. C. Pyrophyllite (light, fine-grained material) replacing quartz. Crossed polars. D. Euhedral crystals of diaspore and pyrophyllite (light, fine-grained material). Crossed polars. E. Stage II silicification (uncrossed polars) showing veinlets of clear silica crosscutting cloudy quartz and replacing kaolinite in phenocryst sites. F. Stage II silicification. Uncrossed polars. Note the boundaries between the clear and cloudy quartz. G. Same field of view as F, but under crossed polars. The black outline marks the boundaries of the phenocryst site occupied by clear silica in F. H. Backscattered electron image of calaverite with Zn tennantite filling site between two pyrite grains and filling microfracture in a pyrite grain. I. Pyrophyllite (light material) filling cracks between sphalerite and crosscutting microcrystalline quartz. (Crossed polars). Abbreviations: Al = (natro)alunite, Au-Te = calaverite, Di = diaspore, Ka = kaolinite, P = pyrophyllite, Py = pyrite, Qz = quartz, Sp = sphalerite, Ten = Zn tennantite.

3.1–9.6), Pb-bearing sulfosalts (with compositions close to As-bearing bournonite, zinckenite, and boulangerite), stibnite, and galena, which occur either as inclusions or as rims or fracture fillings in pyrite, enargite, or sphalerite.

Gold is found in the veins as calaverite with minor silver and copper (<5 wt %), which occurs as blebs in Zn-bearing tennantite which fills fractures in vein pyrite (Fig. 5H) or interstices between pyrite grains. Some calaverite is associated with a mineral having a composition close to As-bearing bournonite as blebs in tennantite. Calaverite also occurs as discrete inclusions, less than 10 μm in diameter, in pyrite. Although not yet observed at Monte Negro, Au-rich electrum along pyrite growth zones in sulfide veins is of primary importance at the Moore orebody (Kesler et al., 1985). Silver-bearing phases observed in the veins include Zn-bearing tennantite (0.75–1.73 wt % Ag), enargite (0.02–0.13% Ag), and Pb-bearing sulfosalts (up to 0.53% Ag).

Interstices between sulfides and the centers of some veins contain feathery, plumose quartz and/or extremely fine grained, milky chert, both of which are probably recrystallized metastable silica. Barite is

present locally in the vein centers or as rims on pyrite grains. Pyrophyllite, which is often present in the veins, appears to have postdated sulfide mineralization, where it fills cracks between sulfide grains and has replaced the vein silica (Fig. 5I). The presence of this pyrophyllite shows clearly that advanced argillic alteration persisted through vein emplacement and sulfide formation and indicates that the veins and advanced argillic alteration resulted from the same fluid.

Distribution of precious metals

Ore and selected rock assays were used to obtain additional information on the mineralogy, distribution, and paragenesis of Au and Ag at Monte Negro, and to determine how precious metal grades relate to stages and types of alteration at Monte Negro. Tellurium and gold assays from diamond drill core (Fig. 6A) show a positive correlation. Most assays plot above the line representing the Te/Au mass ratio of calaverite, indicating the presence of excess Te. Trace Te detected in enargite from Monte Negro (up to 0.03 wt %) is not abundant enough to account for the excess Te. Although not yet detected at Monte Negro, native tellurium, hessite (Ag_2Te), Au-Ag tellurides (with compositions close to krennerite), and copper tellurides have been observed at the Moore orebody (Kesler et al., 1981). The positive correlation between Au and Ag (Fig. 6B) suggests that electrum also hosts precious metals at Monte Negro, despite the scarcity of observations of electrum.

Geologic cross sections with precious metal grade distributions (Fig. 4D–E) show that Au and Ag mineralization is relatively restricted in the spilite and spreads out laterally in the overlying sedimentary rocks. Most high grades occur in the sedimentary rocks, near the neck of the system, although high Au and Ag grades and significant deep Ag mineralization in spilite in the southern part of the section (DDH 235) appear to be separate from the main mushroom-shaped orebody. The cross sections also show that Au and Ag mineralization is restricted to areas of advanced argillic alteration; areas exhibiting only pre-stage I seawater alteration are barren.

The possibility that sulfide veins carried the bulk of the Au at Monte Negro (Kesler et al. 1981) was tested with vein assays used in conjunction with bulk assays and measurements of vein densities from four core holes. The bulk interval grade (IG) can be calculated from the vein density (VD), vein grade (VG), and wall-rock grade (WG) for a given interval by the equation:

$$IG = (5/3)(VD)(VG) + (1 - (5/3)(VD))(WG) \quad (1)$$

(where 5/3 converts vein density from a volume percent to a weight percent, assuming a 5-g/cm^3 density for sulfide vein material, since >90% of the veins contained >90% pyrite, and 3 g/cm^3 for wall rock, based on density measurements discussed below). If the bulk interval grade (IG) is measured independently, eq (1) can be rearranged and used to estimate wall-rock grade and the percentage of gold and silver contributed by the veins.

The results (Table 2) show that, on average, stage II gold-bearing sulfide veins contributed 40 percent of the Au and 47 percent of the Ag in the Monte Negro ore, indicating that there is significant wall-rock Au and Ag. The average measured vein grade for the four holes used in this test is 21.1 ppm Au and 160.8 ppm Ag, yielding an Ag/Au ratio of 7.6. The

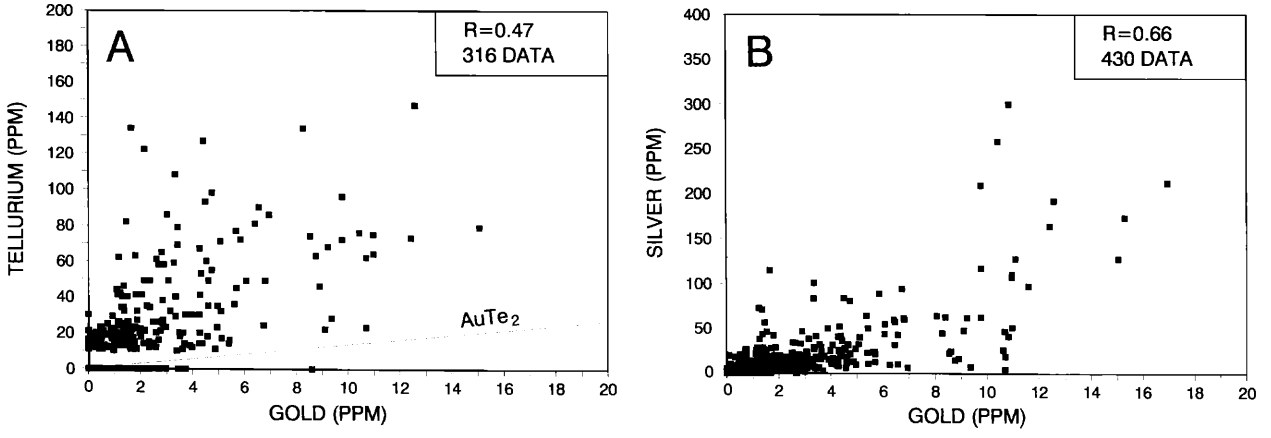

FIG. 6. A. Correlation plot of tellurium and gold assays in areas of advanced argillic alteration. Tellurium assays are from 10-m core intervals and gold assays are 10-m averages of 2-m core interval assays. Line represents the Te/Au wt ratio in calaverite. Assays under the detection limit of 10 ppm for Te is shown as 0 ppm. B. Silver versus gold within areas of advanced argillic alteration. Silver assays are 10-m averages of 2-m core interval assays.

TABLE 2. Vein and Wall-Rock Grade Estimates, Monte Negro

Hole no.	Avg vein density	Avg vein gold grade	Avg bulk gold grade	Avg percent gold in vein	Estimated wall-rock gold grade	Avg gold grade in nonveined 2-m intervals	Avg vein silver grade	Avg bulk silver grade	Avg percent silver in vein	Estimated wall-rock silver grade	Avg silver grade in nonveined 2-m intervals	No. of vein samples	No. of nonveined 2-m intervals
	(%)	(ppm)	(ppm)	(%)	(ppm)	(ppm)	(ppm)	(ppm)	(%)	(ppm)	(ppm)		
DDH195	1.9	21.0	3.5	19	2.8	2.5	130.1	11.0	37	6.9	8.9	57	30
DDH197	9.0	31.2	10.1	46	5.5	4.3	602.0	136.9	66	46.4	3.9	33	6
DDH206	5.3	25.9	3.2	72	0.9	2.6	140.7	13.8	91	1.3	9.1	102	7
DDH225	4.5	6.0	2.0	22	1.6	4.9	23.6	9.2	19	7.4	3.7	39	4
Four hole averages													
Sediments	4.3	28.0	4.7	42	2.7	3.3	252.5	26.3	68	8.4	9.1	81	31
Spilite	4.5	17.8	3.4	39	2.1	2.3	122.4	24.4	38	15.2	5.2	150	16
Total	4.4	21.1	3.8	40	2.3	3.0	160.8	25.0	47	13.2	7.8	231	47

Vein densities were determined using the equation of Haynes (1984), multiplied by vein thickness, which results in the volume percent of the rock that is veined

measured vein density data show no significant variation with rock type (spilite or sediment), depth, or hole location, although they are slightly higher in silicified rock (4.9%) than in nonsilicified rock (3.6%). The average calculated wall-rock grade using eq (1) for the four holes is 2.3 ppm Au and 13.2 ppm Ag, giving an Ag/Au ratio of 5.7. The higher Ag/Au ratio in the veins reflects the presence of Ag-bearing sulfosalts in the veins and their general absence in the wall rock. The estimated Au wall-rock grade of 2.3 ppm (for the 4 holes) is supported by assays of nonveined 2-m intervals (from the 4 holes), which have an average Au grade of 3.0 ppm. The estimated Ag wall-rock grade of 13.2 ppm (for the 4 holes) is not as well supported by assays of nonveined 2-m intervals (from the 4 holes), which have an average Ag grade of 7.8 ppm.

Attempts were made to correlate estimated wall-rock grade with alteration type. Estimated wall-rock grades (0.6 ppm Au, 3.5 ppm Ag) for an interval in DDH195 that contains the stage I alunite zone with minimal stage II overprinting are low and indicate that little Au or Ag was deposited during formation of the stage I alunite zone (Fig. 4B, D, E). Estimated wall-rock grades in intervals with well-developed stage II pyrophyllite formation in the four holes are also low (<2 ppm Au, <10 ppm Ag). Assays of hand samples of massive pyrophyllite alteration, average 0.55 ppm Au (range < 0.1–3.5 ppm, 14 analyses) and 2.5 ppm Ag (range < 0.1–11.8 ppm), support the wall-rock grade estimates and confirm that little, if any, mineralization occurred during formation of stage II massive pyrophyllite. Although remobilization of gold could have occurred during stage II pyrophyllite formation, petrographic evidence supporting equilibrium between pyrophyllite and previously deposited stage I pyrite (which hosts stage I gold) argues against this process.

Wall-rock Au and Ag, therefore, either was deposited during formation of the stage I kaolinite zone or during formation of the stage II silica caps. Based on observations of electrum as inclusions in pyrite that is coeval with stage I kaolinite, the poor correlation between silicification and precious metal grade, and estimated wall-rock grades of 2.1 ppm Au and 15.2 ppm Ag in spilite (Table 2) where stage II silicification is limited, it is most likely that most disseminated Au and Ag were deposited during formation of the stage I kaolinite zone.

Geochemical Environment during Advanced Argillic Alteration and Ore Formation

Calculation of element mobility and water/rock ratios

Chemical analyses and density measurements of spilites (Table 3) were used to estimate the amount

TABLE 3. Abundances of Major Element Oxides (wt%) in Representative Samples

Sample no.	1	2	3	4	5	6	7	8	9	10	11	12	13
SiO_2	56.64	55.91	52.95	45.53	64.94	57.19	47.83	71.61	54.58	64.15	58.77	57.61	52.77
TiO_2	0.72	0.68	0.62	0.52	0.47	0.68	0.91	0.36	0.37	0.46	0.51	0.51	0.53
Al_2O_3	15.83	15.33	14.05	13.04	15.64	17.89	31.97	6.95	18.19	15.63	15.85	18.67	15.69
Fe_2O_3[1]	7.74	9.14	8.42	13.47	8.22	11.78	5.96	9.23	8.34	8.52	12.34	11.36	12.25
MnO	0.13	0.23	0.52	0.01	0.01	0.01	0.01	—	—	—	—	—	—
MgO	4.24	4.72	5.86	0.01	0.01	0.03	0.08	0.05	0.05	0.08	0.04	0.07	0.03
CaO	3.45	3.66	5.11	0.08	0.09	0.13	0.14	0.08	0.10	0.10	0.08	0.09	0.08
Na_2O	4.02	4.91	0.05	1.49	0.01	—	0.01	0.38	0.85	0.21	0.08	0.05	0.74
K_2O	1.12	0.95	0.83	1.39	0.04	0.04	0.15	0.04	1.32	0.02	0.02	0.30	0.95
P_2O_5	0.09	0.09	0.09	0.08	0.15	0.12	0.16	0.07	0.17	0.15	0.15	0.15	0.09
LOI	5.49	3.63	10.51	22.19	8.71	10.70	11.34	7.63	15.40	8.87	11.23	10.29	16.36
Total	99.47	99.25	99.01	97.81	98.29	98.57	98.56	96.40	99.37	98.19	99.07	99.10	99.49
Density[2]	2.80	2.77	2.84	2.99	3.14	3.10	2.82	2.85	3.13	3.04	2.95	3.01	2.99

Sample descriptions: Regional samples: 1 = RD-73-383, spilite, 1.5 km N of Monte Negro orebody (UTM coordinates: 97,000N, 75,400E), represents regional propylitic alteration, unaffected by Pueblo Viejo alteration; 2 = RD-73-538, spilite, 3 km N-NW of Monte Negro orebody (UTM coordinates: 99,400N, 73,400E), represents regional propylitic alteration, unaffected by Pueblo Viejo alteration; Monte Negro samples; 3 = DDH206, 306 m, spilite, cc-chl-qtz-ill-py alteration, 4 m outside advanced argillic alteration; 4 = DDH195, 247 m, spilite, stage I qtz-(nat)alun-py alteration with ca. 5% stage II overprint; 5 = DDH195, 200 m, spilite, stage I qtz-kao-py alteration with >50% stage II pyroph and <10% stage II silica; 6 = DDH206, 302 m, spilite, stage II pyroph replacing qtz; 7 = DDH206, 220 m, spilite, stage II massive pyroph; 8 = DDH195, 90–100 m, spilite, stage II silica replacing stage I kao; 9 = DDH195, 116–126 m, spilite, stage II silica and pyroph overprinting stage I kao zone; 10 = DDH195, 154–162 m, spilite, stage II pyroph and minor silica overprinting stage I kao zone; 11 = DDH195, 204–214 m, spilite, stage II pyroph overprinting stage I kao zone; 12 = DDH195, 218–224 m, spilite, contact between stage I kao and alun zones with ca. 50% stage II pyroph formation; 13 = DDH195, 238–248 m, spilite, stage I alun zone with ca. < 25% stage II overprint

Abbreviations: alun = alunite; cc = calcite, chl = chlorite, ill = illite, kao = kaolinite, LOI = loss on ignition, py = pyrite, pyroph = pyrophyllite, qtz = quartz, nat = natro; — = not detected

Samples were analyzed by X-ray fluorescence spectrometry (XRF) using glass discs and rhodium X-ray excitation; water, sulfur, and carbonate constitute loss on ignition; the low totals for some samples may represent incomplete loss of sulfur (both sulfide and sulfate) on ignition

[1] Fe_2O_3 is total iron as Fe_2O_3

[2] Densities are grain densities (g/cm^3) measured using the ASTM boiling method; assumed to equal bulk density, because the observed porosity of the samples is negligible

of elements mobilized during advanced argillic alteration at Monte Negro. The composite samples used for these tests represent a succession of superimposed alteration types, which provide information on element mobility at a larger deposit size scale. Relative gains and losses of elements during alteration are commonly based on the assumption of constant volume or constant mass of a specific element (Gresens, 1967; Brimhall and Dietrich, 1987; Kerrich et al., 1987). The best evidence for constant volume during alteration at Monte Negro is the preservation of original phenocryst shapes and spatial relationships in the altered spilite (Fig. 5F). Volume increases of only 1 to 5 percent can be attributed to sulfide veining (based on vein density studies of hole DDH195). In contrast, calculations assuming constant Ti, which is the element that appears most likely to have been immobile based on petrographic observations, require volume increases up to 190 percent, which cannot be accommodated by the observed rock textures.

Relative gains and losses of silica, aluminum, and iron for the altered samples, calculated assuming constant volume, are shown in Figure 7. In general silica

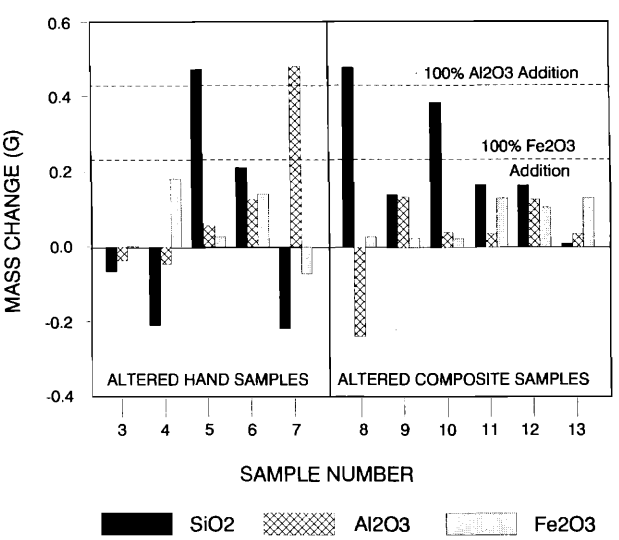

FIG. 7. Bar graph showing additions and subtractions of SiO_2, Al_2O_3, and Fe_2O_3 (in grams, relative to 1 cm^3 of "starting spilite"), in hand samples and composite samples of altered spilite (Table 3), assuming constant volume during alteration. Alteration types for the sample numbers are given in Table 3.

was added to the rocks during alteration, although sample 7 (massive pyrophyllite) shows a significant loss of silica, which is consistent with the replacement of quartz during formation of pyrophyllite, as indicated by petrographic observations (Fig. 5C). Aluminum is often considered to be immobile during hydrothermal alteration (Meyer and Hemley, 1967), but this is obviously not a valid assumption in acid-sulfate systems. Sample 8, which is characteristic of stage II silicification, is substantially enriched in silica with a concomitant decrease in aluminum, supporting the petrographic observation that silica replaced kaolinite in the silicified zones (Fig. 5E). Aluminum addition is expressed by the formation of pyrophyllite. Much of the increases in iron that apparently took place during alteration might be due to pyrite veining (especially in the composite samples). Sample 7 indicates iron was leached during the formation of massive pyrophyllite although no pyrite destructive textures are seen in thin section. Magnesium, calcium, sodium, and potassium, for the most part, were completely removed during advanced argillic alteration.

Minimum concentrations in the fluid that would be required to explain the mass transfer for silica, aluminum, and gold can be calculated for various water/rock ratios (Fig. 8). Average gains and losses of the composite samples were used, because they reflect elemental mass transfer on a deposit scale. A water/rock ratio of 100 requires a minimum average silica concentration of 740 ppm and silica saturation with respect to amorphous silica at 170°C and requires supersaturation with respect to quartz at 300°C. Water/rock ratios were probably somewhat higher, because it is unlikely that fluids could maintain such high silica concentrations during the entire life of the hydrothermal system. These high water/rock ratios (100–1,000) require minimum average aluminum concentrations on the order of 10 to 1,000 ppm and minimum average gold concentrations on the order of 0.1 to 10 ppb (Fig. 8).

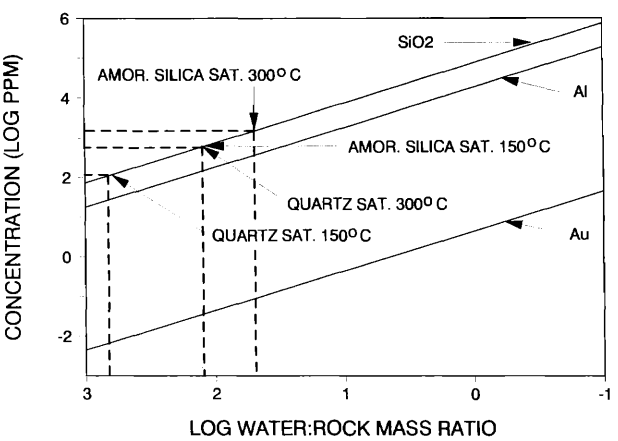

FIG. 8. Estimated water/rock ratios for Monte Negro ore fluids. The three solid lines show how estimated minimum average concentrations required to explain mass transfer of SiO_2, Al, and Au vary with water/rock mass ratio. The concentrations were calculated by determining the average gain or loss of a given element relative to a cm^3 of rock, assuming a rock density of 3 g/cc. Concentrations and water/rock ratios required to explain mass transfer of Fe, Mg, Ca, Na, and K are similar to those of aluminum. The dashed horizontal lines refer to silica saturation (sat.) concentrations for quartz and amorphous (amor.) silica for 150° and 300°C, whereas the dashed vertical lines refer to the water/rock ratios required for silica addition at these silica concentrations.

TABLE 4. Isotopic Composition of Pyrite and Natroalunite

	Monte Negro	Moore
	(‰)	(‰)
Pyrite	−9.5	−3.6
Natroalunite	+20.0	+21.6
$\delta_{py\text{-}nal}$	29.5	25.2
Temperature[1]	184°C	222°C

[1] The aqueous sulfide-sulfate fractionation factor of Ohmoto and Lasaga (1982) and the pyrite-aqueous sulfide fractionation factor of Ohmoto and Rye (1979) were used; fractionation between aqueous sulfate and sulfate in alunite was assumed to be zero (Kusakabe and Robinson, 1977; Ohmoto, 1986)

Temperatures and chemistry of the hydrothermal fluids

Fluid inclusion and isotopic constraints: Possible primary fluid inclusions from silicified spilite and quartz in sulfide veins from Monte Negro homogenized at temperatures of 102° to 136°C and yielded salinities of 0.8 and 3.8 equiv wt percent NaCl (Potter et al., 1978). These results are comparable to data from the Moore orebody, which yielded homogenization temperatures ranging from 135° to 195°C and approximately zero salinities (Kesler et al., 1981). Because much of the quartz in the silicified caps and veins at Monte Negro is probably recrystallized, however, these data probably do not represent the conditions of the fluid during the original deposition of silica (Fournier, 1985; Sander and Black, 1988), and it is necessary to use additional observations to estimate mineralizing temperatures.

Sulfur isotope thermometry on the alunite-pyrite intergrowth shown in Figure 5A indicates a temperature of 184°C for the stage I alunite zone. A temperature of 222°C was calculated from the $\delta^{34}S$ values reported by Kesler et al. (1981) for a similar alunite-pyrite equilibrium intergrowth from the Moore orebody (Table 4). Although kinetics of sulfur isotope exchange between sulfide and sulfate inhibit the attainment of equilibrium below 200°C in most geochemical environments, extremely acid and high sulfur conditions such as prevailed in the alunite zone permit equilibrium to be attained at temperatures as low as 150°C (Ohmoto and Lasaga, 1982). If sulfide-

sulfate equilibrium was not attained at Monte Negro, the 184°C represents a maximum, since attainment of equilibrium would result in a larger fractionation and a lower temperature.

Constraints on temperature and cooling paths from phase equilibria: Additional insights into mineralizing temperatures can be obtained from phase equilibria in the Al_2O_3-SiO_2-H_2O system (Hemley et al., 1980; Fig. 9). Equilibrium between kaolinite and quartz in stage I alteration is limited to temperatures below 260°C, where quartz-saturated solutions react with kaolinite to form pyrophyllite (Hemley et al., 1980). Kaolinite can exist up to temperatures of 285°C if the fluid is undersaturated with respect to quartz, although the previously described silica textures for stage I suggest solutions were supersaturated rather than undersaturated. Therefore, stage I quartz + kaolinite probably formed under temperature conditions shown in Figure 9 by the band above the quartz saturation line (pattern 2). Combined with the 184°C temperature attained from pyrite-alunite thermometry, this observation suggests that most stage I alteration formed at about 200°C.

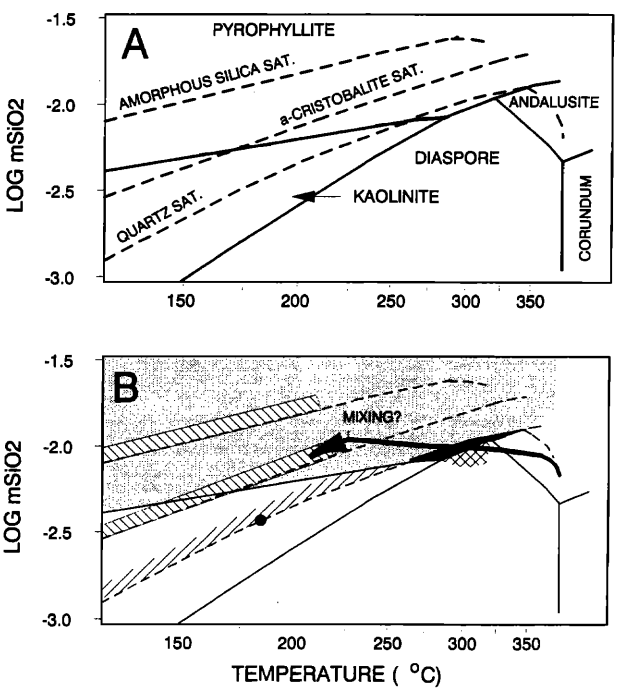

FIG. 9. A. Phase relations in the Al_2O_3-SiO_2-H_2O system (Hemley et al. 1980). Amorphous silica and α cristobalite saturation lines are taken from Helgeson et al. (1978). B. Patterns showing temperature regions for alteration types at Monte Negro. Bold line with arrow shows probable cooling path for stage II fluids.

The coexistence of pyrophyllite and diaspore in stage II alteration limits temperatures to between 285° and 320°C (Fig. 9, pattern 3). Although diaspore can form at lower temperatures in equilibrium with kaolinite, no such texture was observed. The replacement of quartz by pyrophyllite under quartz-undersaturated conditions constrains temperatures to a similar range (260°–340°C, pattern 4). Thus, it appears likely that pyrophyllite formation during stage II alteration and mineralization formed at temperatures of about 300°C, slightly higher than temperatures estimated for stage I. An upper temperature of 220°C for the formation of metastable silica phases such as α cristobalite and amorphous silica can be estimated from observations of active geothermal systems where quartz, not metastable silica phases, has been found to control dissolved silica in all geothermal reservoir waters above 180°C (Arnorsson, 1975; Fournier, 1985) and above 220°C under very acid conditions (J. W. Hedenquist, pers. commun., 1988).

Ascending stage II fluids probably became quartz undersaturated as they cooled through the region of retrograde quartz solubility, shown in Figure 9 where the quartz saturation line bends to a negative slope. A rapidly cooling solution might not have maintained equilibrium saturation with respect to quartz if dissolution rates were slow relative to the rate of fluid migration (Hemley et al., 1980). Such a fluid would move to the left of the quartz saturation line, through the andalusite field, into the diaspore field and eventually into the pyrophyllite field (Fig. 9B). Andalusite has not been observed at either Monte Negro or Moore, although it should be present at depth. It is a common alteration mineral in the gold deposits of the Carolina slate belt (Klein and Criss, 1988) and at the Equity silver deposit (Wojdak and Sinclair, 1984), which are characterized by pyrophyllite alteration.

As upwelling stage II fluids cooled in the pyrophyllite field, acidic conditions would have inhibited silica precipitation (Fournier, 1985) causing silica supersaturation (with respect to quartz, chalcedony, α cristobalite, and possibly even amorphous silica). This could have been maintained until the system was perturbed. Muntean et al., (1988) have suggested from $\delta^{18}O$ data that mixing between mineralizing solutions and ground water in the coarse-grained sediments that overlie the spilite could have been such an event. Note in Figure 4C that the silicified caps are concentrated in the sediments directly overlying the spilite.

Constraints on fluid chemistry from phase equilibria: Phase equilibria, depicted on a log f_{O_2}-pH diagram, provides further constraints on fluid chemistry (Fig. 10). For instance, for stage I fluids at 200°C,

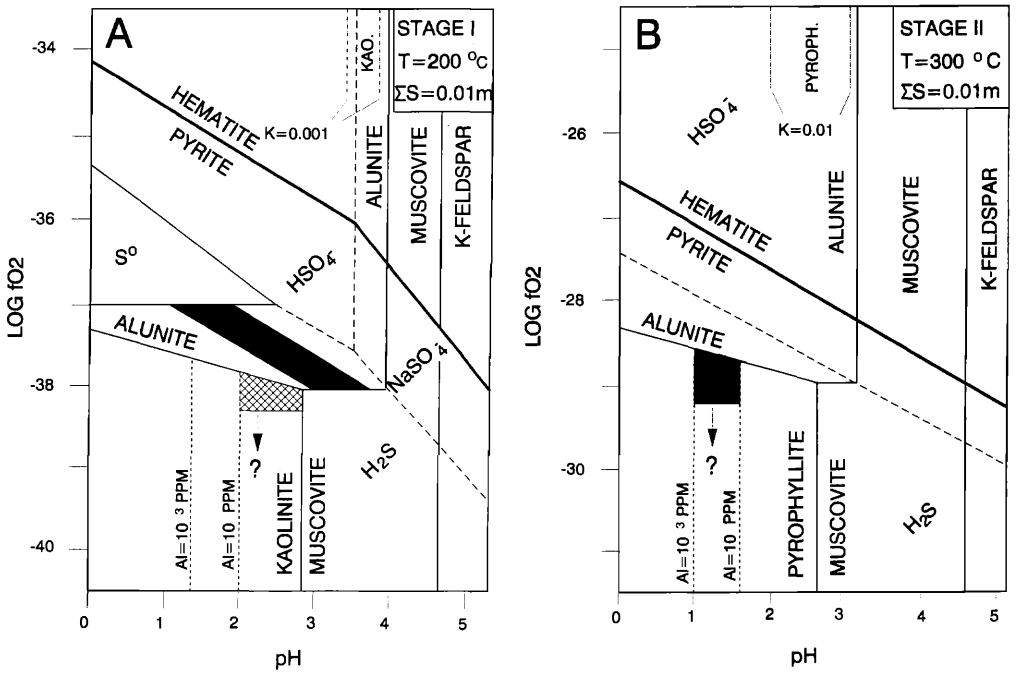

FIG. 10. A. pH-f_{O_2} diagram constructed to represent stage I at 200°C, vapor saturation pressure, quartz saturation, $\Sigma mS = 0.01$, $mK^+ = 0.1$, and an ionic strength of one. The composition of stage I fluids in the alunite zone is the dark band, which represents a sulfate/sulfide ratio of 0.5. Substitution of natroalunite ($mNa^+ = 1.0$) for alunite in this diagram would shift phase boundaries by less than 0.2 pH and log f_{O_2} units. The cross-hatched area represents the kaolinite zone. The vertical total aluminum contours refer to the total concentration of aluminum in the fluid in equilibrium with kaolinite. Aluminum species, included in the calculation, are Al^{+3}, $Al(OH)^{+2}$, and $Al(OH)_2^+$ (concentrations of $Al(OH)_4^-$ and $Al(SO_4)^+$ are insignificant). The phase boundaries labeled "K = 0.001" represent the kaolinite field between the muscovite and alunite fields in the sulfate dominant region at a K^+ concentration of 0.001 *m*. B. A pH-f_{O_2} diagram constructed to represent stage II at 300°C, vapor saturation pressure, quartz saturation, $\Sigma mS = 0.01$, $mK^+ = 0.1$, and an ionic strength of one. The shaded area is the inferred region for stage II pyrophyllite-forming fluids. The vertical total aluminum contours refer to the total concentration of aluminum in the fluid in equilibrium with pyrophyllite. The phase boundaries labeled "K = 0.01" represent the pyrophyllite field between the muscovite and alunite fields in the sulfate dominant region at a K^+ concentration of 0.01 *m*. Data used in constructing the diagram is shown in Appendix A.

total sulfur concentrations greater than 0.01 *m* cause too large a stability field for native sulfur. At total sulfur concentrations less than 0.01 *m*, the alunite field shrinks into the aqueous sulfate dominant field, which disagrees with estimates of sulfate/sulfide ratios in the fluids, as discussed below. A total sulfur concentration of 0.01 *m* was also estimated for stage II. At total sulfur concentrations less than 0.01 *m* unreasonably high iron concentrations (20,000 ppm) are required to maintain pyrite-pyrophyllite equilibrium. At total sulfur concentrations greater than 0.03 *m*, the native sulfur field expands greatly and would have become a dominant phase.

Sulfate/sulfide ratios of the stage I ore fluid can also be estimated from S isotope data, if the bulk isotopic composition of the sulfur is known. It is widely accepted that the source of the acidity and most of the sulfur in hypogene alunite zones is magmatic (Brimhall and Ghiorso, 1983; Bethke, 1984; Giggenbach, 1987; and Stoffregen, 1987). It is unlikely that other sources of sulfur, such as seawater sulfate, could have produced the extremely acid conditions observed in these deposits (Seyfried and Mottl, 1982; Bowers et al., 1985) without the introduction of externally derived acid constituents such as magmatic SO_2 and H_2S. Isotopic analyses of pyrite at Monte Negro fall largely within a $\delta^{34}S$ range of 0 and −10 per mil (Kettler, 1989), supporting the suspected magmatic sulfur source for this system. If the sulfur source is assumed to be largely magmatic with an isotopic ratio of 0 per mil, a sulfate/sulfide ratio of 0.5 can be calculated from the sulfur isotope compositions of the pyrite-alunite pair listed in Table 4 (Ohmoto and Rye, 1979, p. 530). The source of acid constituents and sulfur during stage II was also probably magmatic gases, although the lack of alunite and relatively reduced conditions suggest a decrease in the amount of SO_2.

The upper pH for the stage I alunite zone is limited by the alunite-muscovite phase boundary (pH = 4), and the lower pH is limited by the alunite-native sulfur phase boundary (pH = 1.5). The kaolinite-muscovite phase boundary (pH = 2.9) is the upper pH limit for the kaolinite zone. The lower pH is constrained by contours of total aqueous aluminum concentration that would be in equilibrium with kaolinite. The 10-ppm isopleth (pH = 2) was chosen as the upper aluminum concentration limit, since aluminum appears to have been largely immobile during stage I alteration, as indicated by petrographic observations showing residual aluminum remaining in phenocryst sites as kaolinite. The upper f_{O_2} limit for the kaolinite zone is the kaolinite-alunite phase boundary, while the lower f_{O_2} limit would be the pyrite-pyrrhotite phase boundary (not shown in Fig. 10A).

A pH range of 0.9 to 1.6 for pyrophyllite formation at 300°C during stage II is constrained by total aqueous aluminum concentrations of 1,000 to 10 ppm that would be in equilibrium with pyrophyllite, which is the range of minimum aluminum concentrations required to explain the aluminum addition that occurred during pyrophyllite formation. The upper f_{O_2} limit for stage II fluids is the alunite-pyrophyllite phase boundary. Although the lower f_{O_2} limit is the pyrite-pyrrhotite phase boundary, the lack of textures indicating replacement of alunite by pyrophyllite is evidence that the pyrophyllite-forming fluids were close to equilibrium with alunite and therefore near the alunite-pyrophyllite phase boundary.

Geochemical modeling of gold transport and deposition

Modeling parameters: The observations discussed above indicate that advanced argillic alteration and precious metal mineralization were contemporaneous at Monte Negro. It follows that precious metals are deposited by the same fluids that formed the advanced argillic alteration. This conclusion contrasts with suggestions that precious metals are introduced into acid-sulfate systems when near-neutral, chloride ground waters flood the system after collapse of the acid-sulfate system (Stoffregen, 1987; Berger and Henley, 1989).

In order to further evaluate the capacity of acid-sulfate fluids to transport and deposit gold, we have used the computer programs CHILLER and SOLVEQ (Reed, 1982; Reed and Spycher, 1985; Spycher and Reed, 1989) to model ore-forming processes at Monte Negro. Specific gold-depositing processes that were modeled include sulfidation of wall rock during deposition of stage I disseminated gold mineralization, and boiling, fluid mixing, and cooling to account for gold deposition in stage II veins. Wall-rock reaction was not modeled for stage II because of the previously mentioned lack of alteration selvages around the veins. It should be kept in mind that these calculations do not constitute a comprehensive evaluation of all possible mineralizing processes in acid sulfate deposits and are, instead, an effort to quantify and further test processes that were indicated by our observations at Monte Negro.

TABLE 5. Estimated Initial Fluid Compositions

Component[1] species	Stage I	Stage II	Rationale
Temperature	200°C	300°C	Sulfur isotope thermometry, phase equilibria
pH	2.5	1.5	Phase equilibria
Log f_{O_2}	−38.3	−28.9	Calculated
Log f_{S_2}	−6.6	−4.2	Calculated
I	0.93	0.76	Calculated
Cl	33,123 ppm (1.0 *m*)	33,172 ppm (1.0 *m*)	Assumption
SO_4	8.9 ppm (0.0001 *m*)	99 ppm (0.001 *m*)	Phase equilibria
HCO_3	10,000 ppm	10,000 ppm	Fluid inclusion gas analyses
HS	309 ppm (0.01 *m*)	309 ppm (0.01 *m*)	Phase equilibria
SiO_2[2]	172 ppm	401 ppm	Quartz saturation
Al	0.05 ppm	20 ppm	Phase equilibria
Ca	250 ppm	250 ppm	Mass transfer
Mg	250 ppm	250 ppm	Mass transfer
Fe	1.6 ppm	5,227 ppm	Pyrite saturation
K	3,653 ppm (0.1 *m*)	3,659 ppm (0.1 *m*)	Assumption
Na	19,687 ppm	11,330 ppm	Charge balance
Au[2]	6.9 ppb	119 ppb	Gold saturation

[1] Concentrations of component species refer to total concentrations

[2] Tellurium concentrations of ca. 4.2×10^{-11} ppm at 200°C and 6.4×10^{-8} ppm at 300°C saturate calaverite, given the listed gold concentrations and f_{O_2} values are assuming H_2Te as the dominant aqueous tellurium species (Ahmad et al., 1987).

Total sulfur concentration, sulfate/sulfide ratio, and pH used for the model calculations (Table 5), were derived from the f_{O_2}-pH constraints (Fig. 10), with the fluids being constrained to the kaolinite and pyrophyllite stability fields for stages I and II, respectively. Total aluminum concentrations were determined by saturation with kaolinite (stage I) and pyrophyllite (stage II). Ca and Mg were constrained from minimum concentrations required to explain the mass transfer of these elements during alteration (Fig. 8). Total Cl and K concentrations were estimated at 1 and 0.1 *m*, respectively, as in the f_{O_2}-pH diagrams. The concentration of total carbonate (10,000 ppm) was based on analyses of CO_2 in 1-g samples of vein quartz (Kesler et al., 1986). Silica was determined in both fluids by equilibration with quartz because there is petrographic evidence of quartz-kaolinite equilibrium during stage I, and stage II fluids passed from conditions of silica undersaturation through quartz saturation to silica supersaturation at approximately 300°C. The Na content was determined by charge balance constraints in the solutions. Na was used for this purpose rather than Cl because wall-rock alteration served as both a source (alteration of albite) and sink (formation of natroalunite) for Na, whereas no geologically reasonable source or sink for Cl could be identified. Total Fe and Au were fixed by equilibration with pyrite and gold, respectively. The relatively high Fe content indicated for stage II is supported by evidence for pyrite stability during stage II pyrophyllite formation and Fe assays as high as 30 percent in 2-m drill intervals. Copper and zinc were excluded from the calculations for simplification, although the fact that they form soluble chloride complexes (Barnes, 1979) suggests that their behavior would be similar to that of iron.

The relative importance of the main gold-transporting complexes, $Au(HS)_2^-$ and $AuCl_2^-$, with changes in sulfide and chloride concentrations, is shown in Figure 11 for conditions representing stages I and II. The plots show that during stage I $AuCl_2^-$ could have become the principal aqueous gold species only at improbably low sulfide concentrations (<0.001 *m*) and high salinities (>3 *m*). Under the low pH (1.5), high temperature (300°C) conditions of stage II, however, $AuCl_2^-$ probably predominated over $Au(HS)_2^-$, even to low salinities (m_{Cl^-} = 0.01). Although other aqueous gold species, such as AuHS°, might have been important at low pH, thermodynamic data to evaluate their role at high temperatures are lacking.

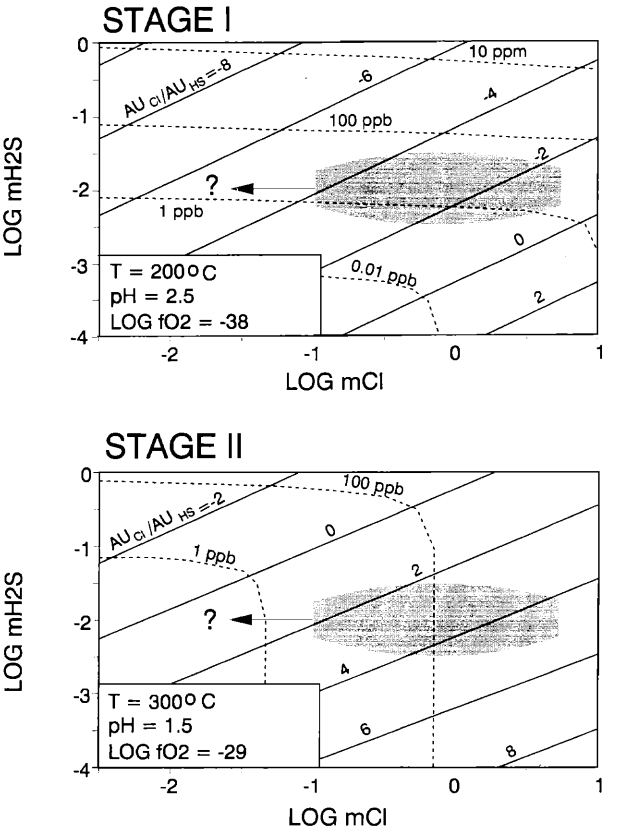

FIG. 11. Relative importance of H_2S and Cl to gold solubility at Monte Negro. Solid contours labeled Au_{Cl}/Au_{HS} show ratios of log molality $AuCl_2^-$/log molality $Au(HS)_2^-$, and dashed contours show variation in total dissolved gold. Shaded regions represent the conditions inferred for stage I and II fluids and represent kaolinite- and pyrophyllite-forming fluids, respectively (Fig. 10). Limits on H_2S are discussed in the text; upper m_{Cl^-} limit is taken from maximum salinities (5.3 *m*; Heald et al., 1987) observed in fluid inclusions from other acid-sulfate deposits. Gold solubility data are from Helgeson (1969) and Shenberger and Barnes (1989). Ionic strength was assumed to equal m_{Cl^-}. Under the conditions listed, H_2S is the dominant aqueous sulfur species for both stages I and II.

Reaction progress models and results for stage I: As discussed above, petrographic and assay data suggest that sulfidation of iron-bearing wall-rock minerals, including siderite, during the formation of the kaolinite zone during stage I caused deposition of large amounts of low-grade gold (Kettler, 1989). To test this possibility, we reacted the stage I fluid (Table 5) with spilite having the average composition of analyses 1 and 2 in Table 3. In the calculation, spilite was added to the stage I fluid at 200°C in increments of 0.1 g until advanced argillic alteration ceased to form. Calculations, which were carried out for an open system, show that 3.0×10^{-6} g of gold were deposited to produce a rock grading 2.9 ppm Au and containing an average alteration mineralogy of 41.1 percent quartz, 19.7 percent pyrite, 35.0 percent kaolinite, and 4.2 percent muscovite. Advanced argillic alteration ceased to form (muscovite formed instead of kaolinite) after 1.1 grams of spilite were added to the fluid at a fluid/rock mass ratio of 973, similar to the high ratios deduced above from whole rock analyses.

Pyrite formed by the sulfidation of ferrous iron by the reaction:

$$4FeO + HSO_4^- + 7H_2S + H^+ = 4FeS_2 + 8H_2O. \quad (2)$$

The consumption of hydrogen ion, sulfate, and sulfide in this reaction caused an increase in pH and decreases in the oxidation state and concentration of aqueous sulfide (Fig. 12). The oxidation state decreased because sulfur was consumed at a sulfate/sulfide molar ratio of 1/7 in eq (2), whereas the initial stage I fluid had a ratio of 1/100 (Table 5). The decrease in aqueous sulfide and oxidation state caused by the reaction in eq (2) caused gold to precipitate by the sulfidation-reduction reaction:

$$16FeO + 8Au(HS)_2^- + 3HSO_4^- + 13H_2S + 11H^+ = 16FeS_2 + 8Au + 28H_2O. \quad (3)$$

This reaction consumed sulfur at a sulfate/sulfide molar ratio of 3/13, resulting in gold deposition accompanied by a sharp decrease in the oxidation state (Fig. 12). With continued reaction with wall rock, gold ceased to precipitate, however, because increasing pH stabilized the gold bisulfide complex to a greater degree than the decreasing total sulfur concentrations destabilized it.

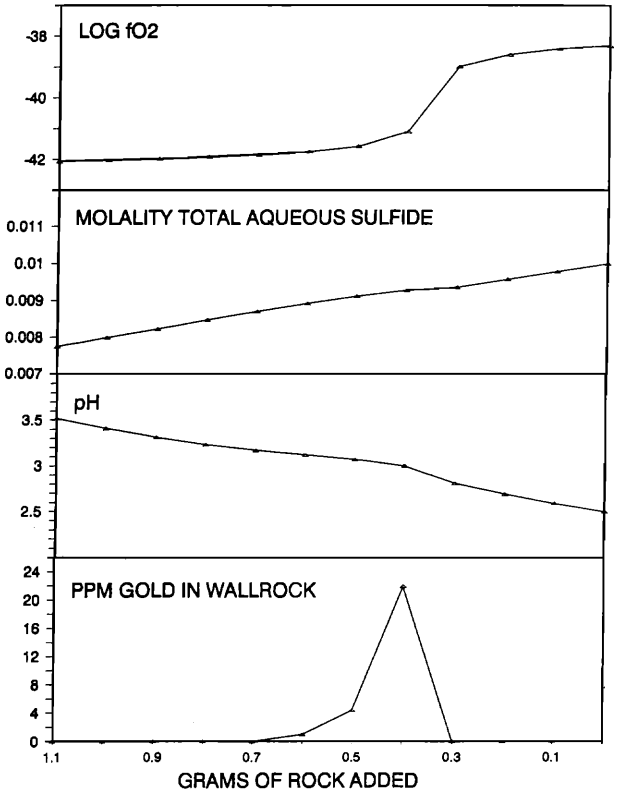

FIG. 12. Results of CHILLER run modeling sulfidation during stage I, showing change in log f_{O_2}, molality of total aqueous sulfide, pH, and gold grade in wall rock as grams of spilite are added to the stage I fluid (Table 5). The sulfidation run was stopped after 1.1 grams of spilite were added when kaolinite ceased to form.

Geologic models and results for stage II: Calculations to compare the efficiency of cooling, fluid mixing, and boiling as causes of gold deposition in stage II veins was also carried out for open systems, although the boiling calculation was closed to escape of gases. Fluid mixing was modeled by mixing the 300°C parent fluid with ground water represented by pure water at 25°C. Quartz has not been observed in stage II veins and was suppressed (e.g., not allowed to precipitate) in all the model runs. This is further supported by experimental data indicating quartz precipitates very slowly in acid solutions (Fournier, 1985), as discussed above. Other metastable silica phases were suppressed above 220°C, the previously noted upper temperature limit of these phases in active geothermal systems.

Results of modeling the stage II fluid indicate that although all three processes deposited gold in the veins, they produce distinctive vein mineralogies and textures. For instance, cooling and mixing would deposit large amounts of pyrite in the veins (85.1% for mixing and 67.8% for cooling) and essentially the same amount of gold (9.3×10^{-5} g), indicating that cooling played a more important role than dilution of chloride in causing gold precipitation. Mixing did not cause significant deposition of silica (the lack of which is characteristic of the vein mineralogy) because the fluid did not reach sufficient levels of supersaturation with silica. In contrast, boiling precipitated only gold until 220°C, where chalcedony was allowed to precipitate. Pyrite did not form during boiling because aqueous sulfide was lost to the gas phase (Fig. 13). Although $AuCl_2^-$ was the dominant aqueous gold species and the chloride content increased with boiling (Fig. 13), gold deposition resulted from the decreased solubility of gold as the temperature dropped. Note that pH decreased during boiling (Fig. 13). This curious feature, which contrasts with the common view that pH increases during boiling by loss of CO_2, which is derived by the following reaction:

$$HCO_3^- + H^+ = H_2O + CO_2(g). \quad (4)$$

At a pH of 2.5, essentially all of the dissolved carbonate is in the form of H_2CO_3, and there is only a negligible amount of HCO_3^- in the fluid, which makes pH increases due to eq (4) insignificant relative to pH decreases due to disassociation of weak acids during cooling (Drummond and Ohmoto, 1985; Reed, 1989).

These results suggest that a combination of the processes modeled here was required to produce the observed gold-bearing stage II veins. Of particular importance in this regard is the observation that much

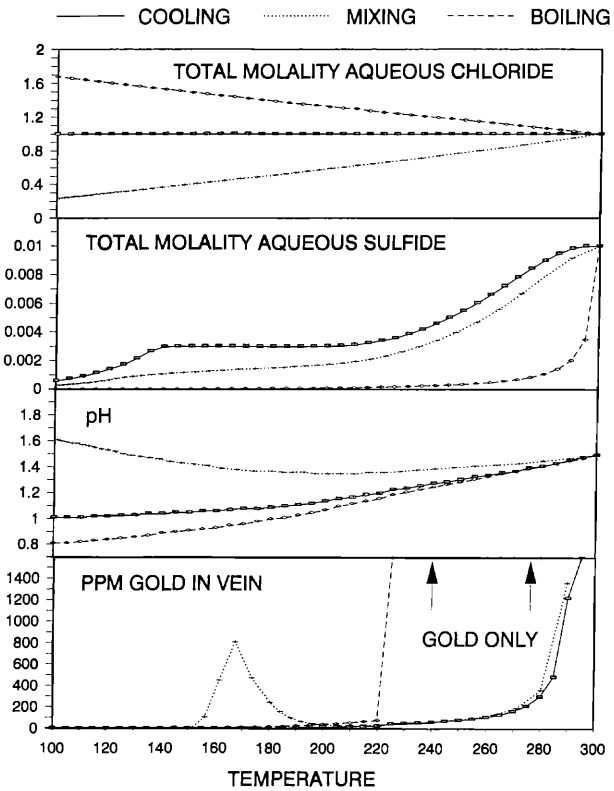

FIG. 13. Results of Stage II CHILLER runs, showing change in molality of total aqueous chloride, molality of total aqueous sulfide, pH, and gold grade in the veins with a temperature decrease. Boiling was modeled as an isoenthalpic process. Only gold was deposited in the boiling run until 220°C, at which point chalcedony was allowed to precipitate. The hump in the gold grades in the mixing run is due to a maximum of the pyrite solubility at ca. 170°C. The cooling run produced 9.3×10^{-5} g of gold in a vein consisting 67.8% pyrite, 31.4% chalcedony, 0.8% graphite, and 101 ppm gold. The fluid mixing run produced 9.3×10^{-5} g of gold in a vein consisting of 85.1% pyrite, 14.1% chalcedony, 0.8% graphite, and 135 ppm gold. The boiling run produced 9.4×10^{-5} g of gold in a vein consisting of essentially 100% chalcedony and 393 ppm gold.

gold in the Moore orebody is found along growth zones in pyrite, as discussed above. The gold-bearing zones apparently formed when pyrite was not being deposited, and they account for much of the gold in the deposit. According to the calculations discussed here, this gold could have been deposited by boiling, whereas much of the intervening pyrite might have been deposited, with or without gold, by cooling and/or mixing. Boiling during stage II could have been caused by hydrofracturing of the silica cap, which would have caused a sudden release of pressure and flashing of the fluid under superisoenthalpic conditions (Reed and Spycher, 1985; Spycher and Reed, 1989). Self-sealing and hydrofracturing are common in active geothermal systems (Muffler et al., 1971; White et al., 1971; Henley and Ellis, 1983) and are widely thought to be the cause of hydrothermal breccias in other epithermal deposits (Berger and Eimon, 1983; Hedenquist and Henley, 1985).

Important Factors in Grade Development at Pueblo Viejo

It is apparent from these observations that several factors were important in making the Monte Negro orebody economically attractive. The first, and possibly most important one, was localization of the hydrothermal system in a maar-diatreme complex that formed by explosive volcanism. The maar-diatreme complex undoubtedly had a high porosity and permeability, especially around its margins, that facilitated circulation of a shallow hydrothermal system. Deeper diatreme permeability could have provided an avenue by which gases and other components from subjacent magma mixed with these waters. Although the quantitative importance of such magmatic contributions is difficult to estimate, Symonds et al. (1987) reported that gases from the Merapi volcano in Indonesia may be enriched in gold by a factor of 10^4 to 10^5 relative to the magma.

The second, third, and fourth important processes are intimately related and represent critical stages in the history of mineralization and alteration at Monte Negro. The second process was clearly sulfidation of wall rock and associated disseminated gold deposition during stage I advanced argillic alteration. Gold grades produced by this process were marginal from an economic standpoint, but they provide a much better background than barren rock to be cut by stage II gold-bearing veins. For instance, using the data in Table 3, Monte Negro, with all the veins removed, would still contain about 34.4 million metric tons of ore grading 2.3 ppm (78 million g of Au). This important background concentration was upgraded by the third important process, which was the formation of stage II veins. The data in Table 3 indicate that although these veins may contain only about 2.7 million metric tons of ore, they have an average grade of 21.1 ppm Au and contain 57 million g of Au, clearly underscoring their importance in making Monte Negro a world-class gold deposit. The fact that stage II took place at a higher temperature than stage I suggests further that waxing systems are more important than waning systems in developing grade and tonnage in acid-sulfate systems. Fluids from higher temperature, waxing stages can carry more gold and have the potential to concentrate earlier, low-grade mineralization. At Monte Negro, these stage II fluids also remobilized silica, causing formation of the silica caps, which actually merits recognition as the final important process in development of mineable grade at Monte Negro. The silica caps apparently sealed the upper part of the hydrothermal system, which caused

hydrofracturing and formation of the high-grade stage II veins. The caps also protected the deposit from rapid erosion during later uplift and exposure.

It follows from these generalizations that exploration for similar systems should focus on areas of explosive volcanism in relatively mafic volcanic rock. The lack of magmatic maar-diatreme complexes in most basaltic terranes and the absence of iron-rich rock in most rhyolitic terranes suggests that the most favorable terranes would be andesitic island-arc volcanic zones. Within individual zones of alteration, attention should focus on areas with pervasive, rather than vein-controlled, alteration in which evidence can be found for wall-rock gold values. Particular attention should be given to zones in which successive hydrothermal events have overprinted this wall-rock gold with higher grade vein-hosted gold. If the form of alteration at Pueblo Viejo can be used as a general guide, it should be found that acid sulfate alteration zones expand in size upward and that their size and grade are enhanced at areas of increased porosity, such as the spilite conglomerate contact at Monte Negro.

Acknowledgments

Thanks go to Rosario Dominicana, S.A., especially Michael Seaward, for travel, field, and logistical support at Pueblo Viejo. Special thanks go to Mark Reed for his generosity in allowing the use of his computer programs SOLVEQ and CHILLER and for his comments on an earlier draft of the manuscript. Discussions with R. Kettler, C. Alpers, R. Loucks, R. Seal, A. Arribas, J. O'Neil, E. Essene, and J. Hedenquist proved invaluable in completing this project. Reviews from two *Economic Geology* referees proved to be very helpful. This research was supported financially by National Science Foundation grant EAR-8607021 awarded to SEK and Phillip Meyers. The senior author was supported by a National Science Foundation graduate fellowship. The scanning electron microscope and electron microprobe at the University of Michigan were made available by NSF grants BSR-83-14092 and EAR-82-12764, respectively.

August 17, 1989; August 27, 1990

REFERENCES

Ahmad, M., Solomon, M., and Walshe, J. L., 1987, Mineralogical and geochemical studies of the Emperor gold telluride deposit, Fiji: ECON. GEOL., v. 82, p. 345–370.

Arnorrson, S., 1975, Application of the silica geothermometer in low-temperature hydrothermal areas in Iceland: Am. Jour. Sci., v. 275, p. 763–784.

Barnes, H. L., 1979, Solubilities of ore minerals, *in* Barnes H. L., ed., Geochemistry of hydrothermal ore deposits: New York, Wiley Intersci., p. 404–460.

Barton, P. B. Jr., and Skinner, B. J., 1979, Sulfide mineral stabilities, *in* Barnes, H. L. ed., Geochemistry of hydrothermal ore deposits: New York, Wiley Intersci., p. 278–403.

Berger, B. R., and Eimon, P., 1983, Conceptual models of epithermal precious metal deposits, *in* Shanks, W. C. III, ed., Cameron volume on unconventional mineral deposits: New York, Am. Inst. Mining Metall. Petroleum Engineers, p. 191–205.

Berger, B. R., and Henley, R. W., 1989, Advances in the understanding of epithermal gold-silver deposits, with special reference to the western United States: ECON. GEOL. MON. 6, p. 405–423.

Bethke, P. M., 1984, Controls on base and precious metal mineralization in deeper epithermal environments: U. S. Geol. Survey Open File Rept. 84-890, 14 p.

Bowers, T. S., Von Damm, K. L., Edmond, J. M., 1985, Chemical evolution of mid-ocean ridge hot springs: Geochim. et Cosmochim. Acta, v. 49, p. 2239–2252.

Bowin, C. O., 1966, Geology of the Central Dominican Republic: Geol. Soc. America Mem., v. 98, p. 11–84.

Brimhall, G. H, Jr., and Dietrich, W. E., 1987, Constitutive mass balance relations between chemical composition, volume, density, porosity, and strain in metasomatic hydrochemical systems: Results on weathering and pedogenesis: Geochim. et Cosmochim. Acta, v. 51, p. 567–587.

Brimhall, G. H, Jr., and Ghiorso, M. S., 1983, Origin and ore-forming consequences of the advanced argillic alteration process in hypogene environments by magmatic gas contamination of meteoric fluids: ECON. GEOL., v. 78, p. 73–90.

Drummond, S. E., and Ohmoto, H., 1985, Chemical evolution and mineral deposition in boiling hydrothermal systems: ECON. GEOL., v. 80, p. 126–147.

Fournier, R. O., 1985, The behavior of silica in hydrothermal solutions: Rev. Econ. Geology, v. 2, p. 45–60.

Giggenbach, W. F., 1987, Redox processes governing the chemistry of fumarolic gas discharges from White Island, New Zealand: Appl. Geochemistry, v. 2, p. 143–161.

Gresens, R. L., 1967, Composition-volume relations of metasomatism: Chem. Geology, v. 2, p. 47–65.

Haynes, F. M., 1984, Vein densities in drill core, Sierrita porphyry copper deposit, Pima County, Arizona: ECON. GEOL., v. 79, p. 755–758.

Heald, P., Foley, N. K., and Hayba, D. O., 1987, Comparative anatomy of volcanic-hosted epithermal deposits: Acid-sulfate and adularia-sericite types: ECON. GEOL., v. 82, p. 1–26.

Hedenquist, J. W., and Henley, R. W., 1985, Hydrothermal eruptions in the Waiotapu geothermal system, New Zealand: Origin, breccia deposits, and effect on precious-metal mineralization: ECON. GEOL., v. 80, p. 1640–1668.

Helgeson, H. C., 1969, Thermodynamics of hydrothermal systems at elevated temperatures and pressures: Am. Jour. Sci., v. 267, p. 729–804.

Helgeson, H. C., Delaney, J. M., Nesbitt, H. W., and Bird, D. K., 1978, Summary and critique of the thermodynamic properties of rock-forming minerals: Am. Jour. Sci., v. 278-A, p. 1–229.

Hemingway, B. S., Haas, J. L., Jr., and Robinson, G. R., Jr., 1982, Thermodynamic properties of selected minerals in the system Al_2O_3-CaO-SiO_2-H_2O at 298.15 K and 1 Bar (10^5 pascals) pressure and at higher temperatures: U.S. Geol. Survey Bull. 1544, 70 p.

Hemley, J. J., Montoya, J. W., Marinenko, J. W., and Luce, R. W., 1980, Equilibria in the system Al_2O_3-SiO_2-H_2O and some general implications for alteration-mineralization processes: ECON. GEOL., v. 75, p. 210–228.

Henley, R. W., and Ellis, A. J., 1983, Geothermal systems, ancient and modern: Earth-Sci. Rev., v. 19, p. 1–50.

Kerrich, R., Fyfe, W. S., Barnett, R. L., Blair, B. B., and Willmore, L. M., 1987, Corundum, Cr-muscovite rocks at O'Briens Zimbabwe: The conjunction of hydrothermal desilicfication and LIL-element enrichment-geochemical and isotopic evidence: Contr. Mineralogy Petrology, v. 95, p. 481–498.

Kesler, S. E., Russell, N., Seaward, M., Rivera, J., McCurdy, K.,

Cumming, G. L., and Sutter, J. F., 1981, Geology and geochemistry of sulfide mineralization underlying the Pueblo Viejo gold-silver oxide deposit, Dominican Republic: ECON. GEOL., v. 76, p. 1096–1117.

Kesler, S. E., Kettler, R. M., Meyers, P. A., Dunham, K. W., Russell, N., Seaward, M., and McCurdy, K., 1985, Relation between organic material and precious metal mineralization in the Moore orebody, Pueblo Viejo, Dominican Republic: Denver Region Explor. Geologists Soc., Spec. Volume 2, p. 105–110.

Kesler, S. E., Haynes, P. S., Creech, M. Z., Gorman, J. A., 1986, Application of fluid inclusion and rock-gas analysis in mineral exploration: Jour. of Geochem. Explor., v. 25, p. 201–215.

Kesler, S. E., Russell, N., Polanco, J., and McCurdy, K., 1991, Geology and geochemistry of the early Cretaceous Los Ranchos Formation, central Dominican Republic: Geol. Soc. of America Spec. Paper (in press).

Kettler, R. M., 1989, Organic matter in hydrothermal systems: Implications for fluid chemistry and source: Unpub. Ph.D. dissert., Ann Arbor, Univ. Michigan, 215 p.

Klein, T. L., and Criss, R. E., 1988, An oxygen isotope and geochemical study of meteoric-hydrothermal systems at Pilot Mountain and selected other localities, Carolina slate belt: ECON. GEOL., v. 83, p. 801–821.

Kusakabe, M., and Robinson, B. W., 1977, Oxygen and sulfur isotope equibria in the $BaSO_4$-HSO_4-H_2O system from 110° to 350°C and applications: Geochim. et Cosmochim. Acta, v. 41, p. 1033–1040.

Meyer, C., and Hemley, J. J., 1967, Wall rock alteration, *in* Barnes, H. L., ed., Geochemistry of hydrothermal ore deposits: New York, Holt, Rinehart, and Winston, p. 166–235.

Muffler, J. P., White, D. E., and Truesdell, A. H., 1971, Hydrothermal explosion craters in Yellowstone National Park: Geol. Soc. America Bull. 82, p. 723–740.

Muntean, J. L., Kesler, S. E., and Valley, J. W., 1988, Evidence for fluid mixing during mineralization, Monte Negro acid-sulfate Au-Ag deposit, Pueblo Viejo, Dominican Republic [abs.]: Geol. Soc. America Abstracts with Programs, v. 20, p. A301–302.

Ohmoto, H., 1986, Stable isotope geochemistry of ore deposits: Rev. Mineralogy, v. 16, p. 491–556.

Ohmoto, H., and Lasaga, A. C., 1982, Kinetics of reactions between aqueous sulfates and sulfides in hydrothermal systems: Geochim. et Cosmochim. Acta, v. 46, p. 1727–1745.

Ohmoto, H., and Rye, R. O., 1979, Isotopes of sulfur and carbon, *in* Barnes, H. L., ed., Geochemistry of hydrothermal ore deposits: New York, Wiley Intersci., p. 509–567.

Potter, R. W., II, Clynne, M. A., and Brown, D. L., 1978, Freezing point depression of aqueous sodium chloride solutions: ECON. GEOL., v. 73, p. 284–285.

Ransome, F. L., 1909, Geology and ore deposits of Goldfield, Nevada: U. S. Geol. Survey Prof. Paper 66, 258 p.

Reed, M. H., 1982, Calculation of multicomponent chemical equilibria and reaction processes in systems involving minerals, gases, and an aqueous phase: Geochim. et Cosmochim. Acta, v. 46, p. 513–528.

—— 1989, Epithermal boiling with decreasing pH: Selective precipitation of gold and silver versus base metal sulfides [abs.]: Geol. Soc. America Abstracts with Programs, v. 21, p. A350.

Reed, M. H., and Spycher, N. F., 1985, Boiling, cooling, and oxidation in epithermal systems: A numerical approach: Rev. Econ. Geology, v. 2, p. 249–272.

Russell, N., and Kesler, S. E., 1991, Geology of the maar-diatreme complex hosting precious metal mineralization at Pueblo Viejo, Dominican Republic: Geol. Soc. of America Spec. Paper (in press).

Russell, N., Seaward, M., Rivera, J., McCurdy, K., Kesler, S. E., Cloke, P. L., 1981, Geology and geochemistry of the Pueblo Viejo gold-silver oxide ore deposit, Dominican Republic: Inst. Mining Metallurgy Trans., v. 90, sec. B, p. B153–B162.

Sander, M. V., and Black, J. E., 1988, Crystallization and recrystallization of growth-zoned vein quartz crystals from epithermal system implications for fluid inclusion studies: ECON. GEOL., v. 83, p. 1052–1060.

Seyfried, W. E., Jr., and Mottl, M. J., 1982, Hydrothermal alteration of basalt by seawater under seawater-dominated conditions: Geochim. et Cosmochim. Acta, v. 46, p. 985–1002.

Shenberger, D. M., and Barnes, H. L., 1989, Solubility of gold in aqueous sulfide solutions from 150° to 350°C: Geochim. et Cosmochim. Acta, v. 53, p. 269–278.

Siddeley, G., and Araneda, R., 1986, The El Indio-Tambo gold deposits, Chile, *in* Macdonald, A. J., ed., Gold '86: Willowdale, Ontario, Konsult Internat., Inc., p. 445–456.

Sillitoe, R. H., and Bonham, H. F., Jr., 1984, Volcanic landforms and ore deposits: ECON. GEOL., v. 79, p. 1286–1298.

Smith, R. M., and Martell, A. E., 1976, Critical stability constants: New York, Plenum Press, v. 4, 257 p.

Spycher, N. F., and Reed, M. H., 1989, Evolution of a broadlands-type epithermal ore fluid along alternative P-T paths: Implications for the transport and deposition of base, precious, and volatile metals: ECON. GEOL., v. 84, p. 328–359.

Stoffregen, R., 1987, Genesis of acid-sulfate alteration and Au-Cu-Ag mineralization at Summitville, Colorado: ECON. GEOL., v. 82, p. 1575–1591.

—— 1988, An experimental study of alkali exchange between alunite and $(Na,K)_2SO_4$-bearing solutions [abs.]: Geol. Soc. America Abstracts with Programs, v. 20, p. A390.

Stoffregen, R., and Alpers, C. N., 1987, Woodhouseite and svanbergite in hydrothermal ore deposits: Products of apatite destruction during advanced argillic alteration: Canadian Mineralogist, v. 25, p. 201–211.

Symonds, R. B., Rose, W. I., Reed, M. H., Lichte, F. E., and Finnegan, D. L., 1987, Volatilization, transport and sublimation of metallic and non-metallic elements in high temperature gases at Merapi volcano, Indonesia: Geochim. et Cosmochim. Acta, v. 51, p. 2083–2101.

White, D. E., Muffler, J. P., and Truesdell, A. H., 1971, Vapor-dominated hydrothermal systems compared with hot-water systems: ECON. GEOL., v. 66, p. 75–97.

Wodjak, P. J., and Sinclair, A. J., 1984, Equity Silver silver-copper-gold deposit: Alteration and fluid inclusion studies: ECON. GEOL., v. 79, p. 969–990.

Wolery, T. J., 1986, EQ3NR a computer program for geochemical aqueous speciation-solubility calculations: Users guide and documentation: Livermore California, Lawrence Livermore Natl. Lab., 191 p.

APPENDIX

Thermodynamic Data Used to Construct Log f_{O_2}-pH Diagrams

Reaction	Log K 200°C	Log K 300°C	Source
Aqueous sulfur species			
1. $H_2S_{(aq)} + 2O_2 + Na^+ = 2H^+ + NaSO_4^-$	68.01	49.48	1, 2, 3
2. $H_2S_{(aq)} + 2O_2 = HSO_4^- + H^+$	71.3	54.31	1, 2

3. $H_2S_{(aq)} = H^+ + HS^-$	−6.96	−8.06	2
4. $HS^- + 2O_2 + Na^+ = NaSO_4^- + H^+$	74.97	57.54	1, 3
5. $HSO_4^- + Na^+ = H^+ + NaSO_4^-$	−3.31	−4.74	1, 3
Sulfur saturation			
6. $2H_2S_{(aq)} + O_2 = 2S_{(l)} = 2H_2O$	41.00	31.26	1, 2, 4
7. $2H^+ + 2HSO_4^- = 3O_2 + 2S_{(l)} + 2H_2O$	−101.64	−77.36	1, 2, 4
Pyrite-hematite-magnetite equilibria			
8. $4FeS_2 + 15O_2 + 8Na^+ + 8H_2O = 2Fe_2O_3 + 16H^+ + 8NaSO_4^-$	467.72	340.84	1, 3
9. $4FeS_2 + 15O_2 + 8H_2O = 2Fe_2O_3 + 8H^+ + 8HSO_4^-$	494.20	379.48	1, 2
10. $3FeS_2 + 6H_2O = Fe_3O_4 + 6HS^- + 6H^+ + O_2$	−109.17	−97.35	1
11. $4Fe_3O_4 + O_2 = 6Fe_2O_3$	40.49	31.01	1
12. $3FeS_2 + 11O_2 + 6Na^+ + 6H_2O = Fe_3O_4 + 6NaSO_4^-$	340.67	247.88	1, 3
Muscovite-feldspar equilibria			
13. $3KAlSi_3O_8 + 2H^+ = KAl_3Si_3O_{10}(OH)_2 + SiO_{2(qtz)} + 2K^+$	8.18	7.72	1
Alunite-muscovite equilibria			
14. $2KAl_3(SO_4)_2(OH)_6 + 6SiO_{2(qtz)} = 2KAl_3Si_3O_{10}(OH)_2 + 4H^+ + 4HSO_4^-$	−27.04	−22.63	1, 2
15. $2KAl_3(SO_4)_2(OH)_6 + 6SiO_{2(qtz)} = 2KAl_3Si_3O_{10}(OH)_2 + 4H_2S + 8O_2$	−312.34	−239.90	1
16. $2KAl_3(SO_4)_2(OH)_6 + 6SiO_{2(qtz)} + 4Na^+ = 2KAl_3Si_3O_{10}(OH)_2 + 8H^+ + 4NaSO_4^-$	−40.28	−37.87	1, 3
Alunite-kaolinite-muscovite equilibria			
17. $2KAl_3Si_3O_{10}(OH)_2 + 3H_2O + 2H^+ = 3Al_2Si_2O_5(OH)_4 + 2K^+$	4.46		1
18. $2KAl_3(SO_4)_2(OH)_6 + 6SiO_{2(qtz)} + 3H_2O + 2H^+ = 3Al_2Si_2O_5(OH)_4 + 2K^+ + 4H_2S_{(aq)} + 8O_2$	−307.88		1, 2
19. $2KAl_3(SO_4)_2(OH)_6 + 6SiO_{2(qtz)} + 3H_2O = 3Al_2Si_2O_5(OH)_4 + 2H^+ + 2K^+ + 4HSO_4$	−22.58		1, 2
20. $2KAl_3(SO_4)_2(OH)_6 + 6SiO_{2(qtz)} + 3H_2O + 4Na^+ = 3Al_2Si_2O_5(OH)_4 + 4NaSO_4^- + 2K^+ + 6H^+$	−35.82		1, 3
Alunite-pyrophyllite-muscovite equilibria			
21. $2KAl_3Si_3O_{10}(OH)_2 + 6SiO_{2(qtz)} + 2H^+ = 3Al_2Si_4O_{10}(OH)_2 + 2K^+$		3.63	1
22. $2KAl_3(SO_4)_2(OH)_6 + 12SiO_{2(qtz)} + 2H^+ = 3Al_2Si_4O_{10}(OH)_2 + 2K^+ + 4H_2S + 8O_2$		−236.27	1, 2
23. $2KAl_3(SO_4)_2(OH)_6 + 12SiO_{2(qtz)} = 3Al_2Si_4O_{10}(OH)_2 + 2K^+ + 4HSO_4^- + 2H^+$		−19.00	1, 2
24. $2KAl_3(SO_4)_2(OH)_6 + 12SiO_{2(qtz)} + 4Na^+ = 3Al_2Si_4O_{10}(OH)_2 + 4NaSO_4^- + 2K^+ + 6H^+$		−38.32	1, 3
Kaolinite-pyrophyllite saturation			
25.[1] $Al_2Si_2O_5(OH)_4 + 6H^+ = 2Al^{+3} + 2SiO_{2(qtz)} + 5H_2O$	−2.98		1, 5
26.[1] $Al_2Si_4O_{10}(OH)_2 + 6H^+ = 2Al^{+3} + 4SiO_{2(qtz)} + 4H_2O$		−10.44	1, 5
27. $AlOH^{+2} + H^+ = Al^{+3} + H_2O$	2.22	1.35	6
28. $Al(OH)_2^+ + 2H^+ = Al^{+3} + 2H_2O$	4.94	3.10	6
Gold saturation			
29. $Au + H_2S_{(aq)} + HS^- + \frac{1}{4}O_2 = Au(HS)_2^- + \frac{1}{2}H_2O$	9.70	7.55	1, 2, 7
30. $Au + H^+ + 2Cl^- + \frac{1}{4}O_2 = AuCl_2^- + \frac{1}{2}H_2O$	2.23	3.23	2

References: 1 = Helgeson et al. (1978); 2 = Helgeson (1969); 3 = Smith and Martell (1976); 4 = Barton and Skinner (1979); 5 = Hemingway et al. (1982); 6 = Wolery (1986); 7 = Shenberger and Barnes (1989)

[1] The log K values were determined by adding a correction of −6.5 kJ per mole of aluminum to the free energy value reported by Helgeson et al. (1978), as recommended by Hemingway et al. (1982)